minerals

MDPI

Article

Petrogenesis and Metallogenesis of Granitoids in the Yangla Cu-W Polymetallic Deposit, Southwest China: Evidence from Zircon Trace Elements and Hf Isotope

Xinfu Wang [1], Bo Li [1,*], Guo Tang [1,2], Zhen Lei [1] and He Chang [1]

[1] Faculty of Land Resource Engineering, Kunming University of Science and Technology, Kunming 650093, China
[2] Kunming Prospecting Design Institute of China Nonferrous Metals Industry Co., Ltd., Kunming 650051, China
* Correspondence: libo8105@kust.edu.cn; Tel.: +86-159-8718-7981

Abstract: Magmatic zircon tends to present characteristic trends in trace element compositions in response to magma petrogenesis and metallogenesis, such that zircon may provide a window into melt evolution not accessible by whole rock chemistry. The Yangla large Cu deposit is located in the central part of the Jinshajiang Suture Zone, southwest China, constrained between the Jinshajiang and Yangla Faults. In this study, the trace elements and hafnium isotopic compositions of zircons from quartz diorite were studied. Previous published relevant data of Yangla granitoid plutons (i.e., dioritic enclave, granodiorite, and quartz monzonite porphyry) also have been systematically cited and discussed. The result shows that the crystallization temperature and two-stage Hf mode ages (t^{C}_{DM}; the age of the source rocks for the magmas) gradually increased while the oxygen fugacity (fO_2) and $\varepsilon_{Hf}(t)$ values gradually decreased, corresponding to the diorite enclave (~232 Ma), through granodiorite (~208 Ma) and quartz monzonite porphyry (~202 Ma), and to quartz diorite (~195 Ma). It is suggested that four plutons were from the same three-component mixing of upper crust + lower crust + mantle magmas, while the upper crustal metasediments ratios were gradually increased from the early to late stage. The increasing upper crust inputs resulted in higher melting temperatures and compositions of the initial magma. All melts experienced distinct fractional crystallization of apatite, titanite, and amphibole, and the later granite melts experienced higher assimilation and fractional crystallization degrees than the early ones in the evolution processes four stages of intrusive rocks. These Yangla granitoids are the products of large-scale acid magmatic emplacement activities in the Triassic-early Jurassic and have a good metallogenic potential of the Cu-W polymetallic deposit.

Keywords: zircon trace elements; Hf isotope; magmatic genesis; geodynamic setting; metallogenic potential; Yangla Cu-W polymetallic deposit

Citation: Wang, X.; Li, B.; Tang, G.; Lei, Z.; Chang, H. Petrogenesis and Metallogenesis of Granitoids in the Yangla Cu-W Polymetallic Deposit, Southwest China: Evidence from Zircon Trace Elements and Hf Isotope. *Minerals* **2022**, *12*, 1427. https://doi.org/10.3390/min12111427

Academic Editors: Huan Li, Rongqing Zhang, Jie-Hua Yang, Jingya Cao and Stefano Salvi

Received: 9 October 2022
Accepted: 7 November 2022
Published: 10 November 2022

1. Introduction

The Yangla Cu-W polymetallic deposit (YCWPD) (28°51′–28°59′ N, 99°04′–99°07′ E) is located in Deqin County, northwest Yunnan, southwest China, and is one of the representative deposits in the "Sanjiang" Polymetallic Metallogenic Domain (SPMD; Figure 1a,b) [1]. The YCWPD contains ore reserves of 150 Mt Cu @ 1% in the Jinshajiang Suture Zone (JSZ) [1]. Since the discovery of YCWPD in the 1960s, substantial research has been carried out within the Yangla mining district. Fruitful research has been conducted on diagenesis and Cu mineralization, including elucidation of the diagenetic chronology and petro-geochemistry of the Beiwu, Jiangbian, Linong, Lunong, and Tongjige granodiorite plutons [2–6], ore-forming fluid and isotope geochemistry [7,8], isotopic geochronology [8,9], the metallogenic mechanism [8–10], and ore genesis [11,12]. The general consensus is that the YCWPD is genetically associated with the magmatic emplacement and other evolution events of the Jinshajiang Ocean Basin (JOB) in the Late Triassic (~230 Ma). The metallogenic

materials are mainly related to acidic magma and are partly contaminated by the meteoric water and upper crustal sedimentary materials [1,7–9]. The boiling action of hydrothermal fluid accompanied the cooling is the main mechanism of Cu precipitation and enrichment at YCWPD [13]. The YCWPD can be regarded as a composite superimposed genetic deposit, and the mineralization sequence may have undergone the exhalative-sedimentary to skarn-porphyry [12]. Recently, a new (copper-mineralized) quartz diorite was discovered during ore prospecting exploration at the depth (3250 m sections) of the Linong ore block within the YCWPD; the emplacement age, petro-geochemistry and genesis of this new quartz diorite pluton have been well-constrained [13,14], but its magma origin and properties, evolution process, geodynamic setting, and metallogenic potential require further analysis and discussion.

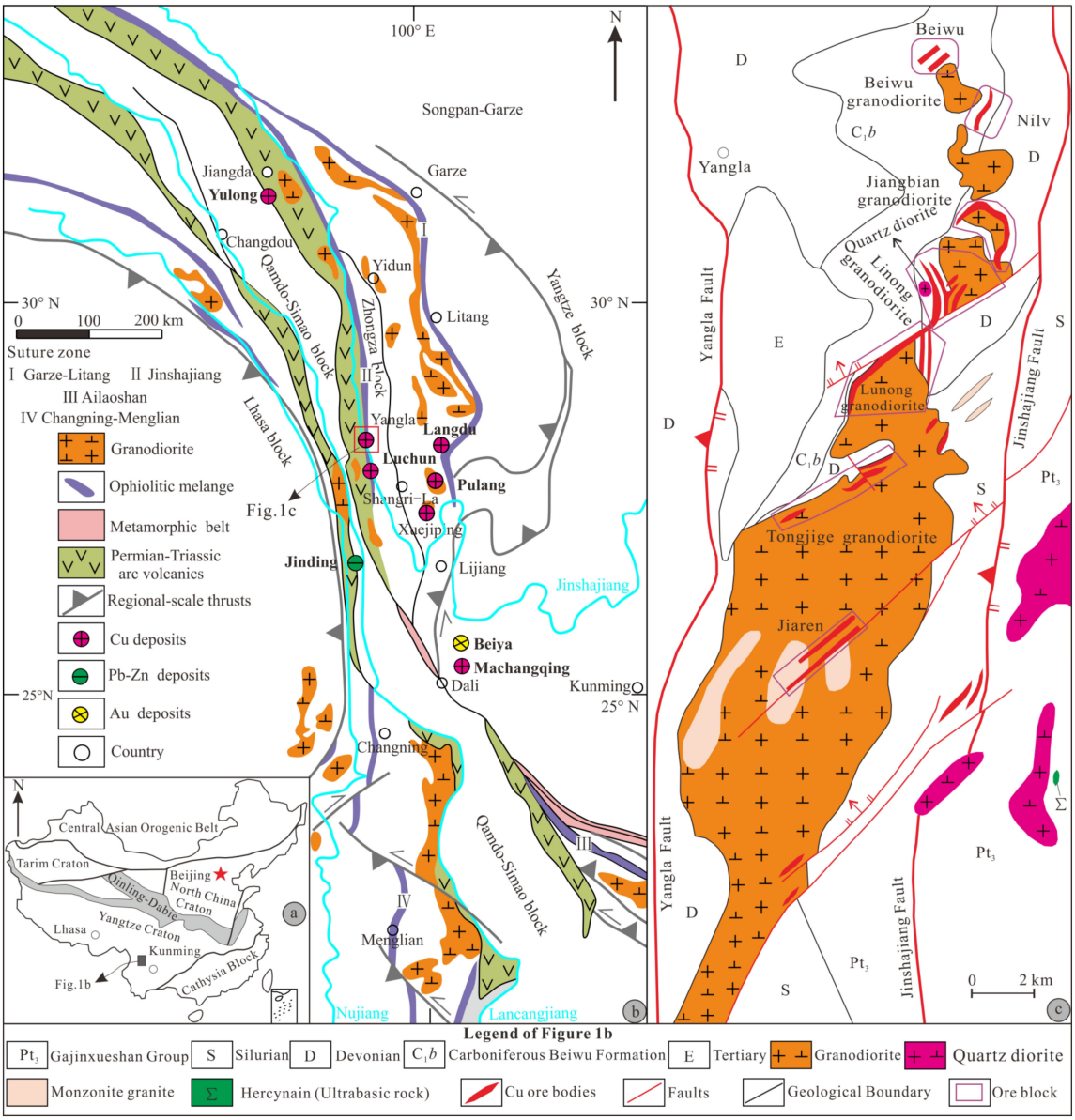

Figure 1. (**a**) Geotectonic framework sketch map of China [2]. (**b**) Regional geological sketch map of the Sanjiang region, southwest China [8]; (**c**) geologic sketch map of the Yangla Cu-W polymetallic deposit, northwest Yunnan, China [1].

Trace elements (i.e., REE) and the hafnium isotopic system of zircon can be regarded as an important provenance indicator for the origin of granites, which can provide a better constraint on the involvement of magmas [3,15–18]. Currently, the trace element compositions

(i.e., REE, Y, Nb, Ta, Ti, U, and Th) of zircon have been widely used to estimate crystallization temperature and oxygen fugacity, discuss assimilation and fractional crystallization and assess metallogenic potential assessment [19–25]. Moreover, hafnium isotopes of zircon have been broadly used to trace the magma source, assemblage sequence, petrogenetic types, tectonic setting, and magmatic evolution, combined with the chronology, oxygen isotope, and other whole-rock isotope data (Sr-Nd-Pb) [2,26,27], such as Yangla granodiorite plutons in Sanjiang region [3,5], Pulang composite granite intrusion in Sanjiang region [28], Dazeshan-Tianzhushan granites in Jiaodong peninsula [27], and Erdene granite in south Mongolia [29].

This study mainly presented the zircon trace elements and Hf isotopic composition of the newly discovered quartz diorite in the YCWPD. Moreover, previously published data (i.e., diagenetic chronology data, zircon trace elements, and Hf isotopic compositions) from granodiorite plutons (Beiwu, Jiangbian, Linong, Lunong, and Tongjige), quartz monzonite porphyry and, dioritic enclaves within the granodiorite, are systematically collected and re-interpreted, and the crystallization temperature, petrology, geodynamic setting, and metallogenic potential of acidic magma are discussed in the YCWPD. Combined with previously published data, this study can not only enrich and systematically establish the origin and evolutionary sequence of acid magma in the Yangla region but also analyze the metallogenic potential of the Yangla granitoids plutons.

2. Geological Setting

The Sanjiang region is a key metallogenic zone in SW China (Figure 1a) [14] and mainly consists of several ophiolite suture zones, a magmatic belt, several microcontinental blocks, and regional thrusts (Figure 1b) [2,7]. Studies have shown that four branches of the Paleo-Tethyan Ocean have been recognized, such as the Garzê-Litang Ocean (suture I in Figure 1b), Jinshajiang Ocean (suture II in Figure 1b), Ailaoshan Ocean (suture III in Figure 1b), and the Changning-Menglian Ocean (suture IV in Figure 1b) [30]. Furthermore, numerous igneous rocks (i.e., Baimaxueshan, Jiaren, and Lincang granitoids) and large to super-large Cu-polymetallic deposits (i.e., Yulong, Yangla, Pulang, and Xuejiping) have been formed and discovered since the Paleozoic to Cenozoic [1,12].

The YCWPD is constrained to the east and west by the regional Jinshajiang and Yangla Faults, respectively. This restricts mining to a narrow N-S-trending region with an area of approximately 12.40 km^2 (Figure 1c). The YCWPD is mainly divided into seven ore blocks (Figure 1c); the Linong is the largest, with proven copper metal reserves of approximately 600,000 tons and average copper content of approximately 1.0% [1,14]. The newly discovered quartz diorite occurs at a depth of the Linong ore block; therefore, this study mainly focuses on the Linong when describing the geological setting.

The Yangla Cu mineralization is closely associated with the spatiotemporal properties and origin of the granitic plutons. The Cu ore bodies are typically produced around acidic intrusions, not only in the surrounding rocks of the outer contact zone but also in the fractured zone and inner contact zone within the plutons [1]. Furthermore, stratigraphic, lithological, and structural controls of the Cu ore body distribution are particularly evident in the YCWPD [31]. The Devonian Jiangbian and Linong formations are important ore-bearing components of the local stratigraphy. Skarn is the main ore-hosting lithology of the YCWPD, followed by altered metamorphic quartz sandstone, sericitic sandy slate, marble, and granodiorite [1,31]. The NNE- and nearly N-S-trending faults and other fracture zones are important ore-controlling or ore-hosting structures [31].

The exposed stratigraphy is mainly dominated by the Silurian (S), Devonian (D), and lower Carboniferous (C_1) units; the Devonian is further divided into a lower sequence (D_1) and a middle-upper sequence (D_{2+3}), which are the main ore-bearing horizons in the Yangla skarn Cu body [11,31]. The Lower Devonian stratigraphy can be further divided into the first (D_1j^1), second (D_1j^2), and third (D_1j^3) sequence of the Jiangbian Formation, whereas the middle-upper Devonian can be further divided into the first ($D_{2+3}l^1$), second ($D_{2+3}l^2$), and third ($D_{2+3}l^3$) sequence of the Linong Formation. The third members (D_1j^3)

of the Jiangbian Formation are the ore-host sequences of JKT1, JKT2, JKT4, and JKT5 ore bodies in the YCWPD. The exposed lithology of the Linong Formation primarily comprises metamorphosed quartz arenite, sericitic sandy-slate, marble, and intruded granodiorite, and its contact zones often exhibit skarnization, silicification, and carbonization, and the main ore body is the KT2 ore-bearing sequence in the YCWPD. The Lower Carboniferous (Beiwu Formation, C_1b) primarily comprises massive basalt, tuff, and sandy slate and outcrops northwest of the YCWPD.

The Yangla mining district has experienced strong tectonic activity and significant fault control of orebodies. The approximately N-S-trending Jinshajiang and Yangla Faults mainly control the regional magmatism and distribution of ore deposits [31,32]. A group of parallel secondary NE-SW-trending normal faults, represented by F4, are also developed in this district, and these faults, together with the Jinshajiang Fault, present a "λ"-shaped structural style in plan-view, which controls the spatial positioning of the pluton and ore bodies. Secondary interlayer faults (mostly dominated by lithologic interfaces) control the morphology of the layered and stratiform-stratoid skarn Cu ore bodies. Fissures in the pluton control the shape of veined Cu orebodies. Late NE-SW- and NW-SE-trending faults, which formed after diagenesis-mineralization cleavage and dislocated the pluton and orebodies, control the spatial positioning and final occurrence of both the pluton and orebodies [31,32].

The intrusive bodies, volcanic rocks, and dikes are widely developed within the YCWPD [1]. The intrusive bodies primarily comprise granodiorite and dioritic enclaves within the granodiorite, quartz monzonite porphyry, and quartz diorite in the YCWPD. Granodiorite comprises the largest exposed area and can be divided into five intrusions from north to south (i.e., Beiwu, Jiangbian, Linong, Lunong, and Tongjige) in the YCWPD, all of which were intruded into the Linong Formation and distributed linearly along the western side of Jinshajiang Fault [2,8]. The granodiorite contains plagioclase, K-feldspar, quartz, hornblende, minor amounts of biotite, and accessory zircon [2]. The granodiorite was primarily formed during the Triassic (~230 Ma) and has been confirmed that closely related to Cu skarn mineralization at the Yangla region [2,3,5,8]. The granodiorite samples are dominantly metaluminous and slightly peraluminous (A/CNK < 1.10), and there is a significant negative correlation between SiO_2 and P_2O_5 [2]. Moreover, there is also a significant positive correlation between SiO_2 and Pb [2]. These granodiorite samples are mainly plotted within the I-S-type granite region in the binary diagram of $K_2O + Na_2O$ vs. 10,000 Ga/Al, Y vs. 10,000 Ga/Al, Zr vs. 10,000 Ga/Al, and Nb vs. 10,000 Ga/Al. However, there were no presented muscovite and cordierite in granodiorite samples and corundum lower than 1.0% in CIPW standard mineral calculation [2–5]. The granodiorite samples were mainly dominated by post-collision granites in the binary-ternary tectonic discrimination diagrams of Nb vs. Y, Ta vs. Yb, Rb vs. Y + Nb, Rb vs. Yb + Ta, and Rb/30-Hf-3 × Ta [2,5]. Therefore, petro-geochemical characteristics show that the granodiorite may belong to the I-type granites and formed in a late- or post-collisional tectonic setting after the closure of JOB [2–5]. The dioritic enclaves (2–10 cm in diameter) preserves transitional or irregular sharp contact relationship with the host granodiorite and presents a porphyritic texture. The phenocrysts are mainly dominated by plagioclase, biotite, hornblende, and K-feldspar [3]. Zircons U-Pb ages of dioritic enclaves are 232 and 238 Ma [3], which are roughly consistent with the chronology and tectonic setting of granodiorite intrusion.

The phenocrysts of quartz monzonite porphyry are mainly dominated by plagioclase, K-feldspar, minor quartz, biotite, and accessory apatite and zircon; it intrudes the third sequence ($D_{2+3}l^3$) of the Linong Formation [3]. The Rb-Sr chronology shows that the emplacement age of petrogenesis is 202 Ma [33], whereas the zircon U-Pb chronology yields ages of 232 Ma and 234 Ma [3]; this suggests that the quartz monzonite porphyry may have formed in the late Triassic, and has similar petro-geochemical characteristics and tectonic setting to the GR [3]. Furthermore, the quartz monzonite porphyry is considered to be genetically related to the porphyry copper orebody (KT1), and it has been suggested that the porphyry copper orebody exists at a depth of Yangla mining district [33].

The quartz diorite occurs in an underground tunnel in 3250 m sections (levels) of the Linong ore block, where it is emplaced within Linong Formation metamorphosed quartz arenite and sericitic-slate (Figures 2–4). The quartz diorite mainly occurred within a NE-SW-trending faults and (or) fractures zone (4~5 m in width and 20~300 m in length), and the contact boundary line show irregular shape between the quartz diorite and Devonian wall-rocks. The petro-geochemical features show that the quartz diorite is relatively enriched in LILEs, depleted in HFSEs, significantly enriched in Pb, and depleted in P [14]. Studies have suggested the quartz diorite may be metaluminous to slightly peraluminous S-type granite and formed in a post-collisional tectonic setting [14]. Zircon U-Pb chronology shows that the crystallization ages of the quartz diorite are 195.3 ± 6.4, 198.40 ± 8.6, and 213 ± 15 Ma (avg. 202 Ma) and indicated it formed in the Late Triassic to Early Jurassic (~195 Ma) [14]. Moreover, plenty of veined, disseminated sulfides (i.e., pyrite, chalcopyrite, and sphalerite) and quartz-calcite veins are developed in the interior fissures of quartz diorite (Figure 3c,d and Figure 4e,f), suggesting that it may be related to Yangla porphyry Cu mineralization.

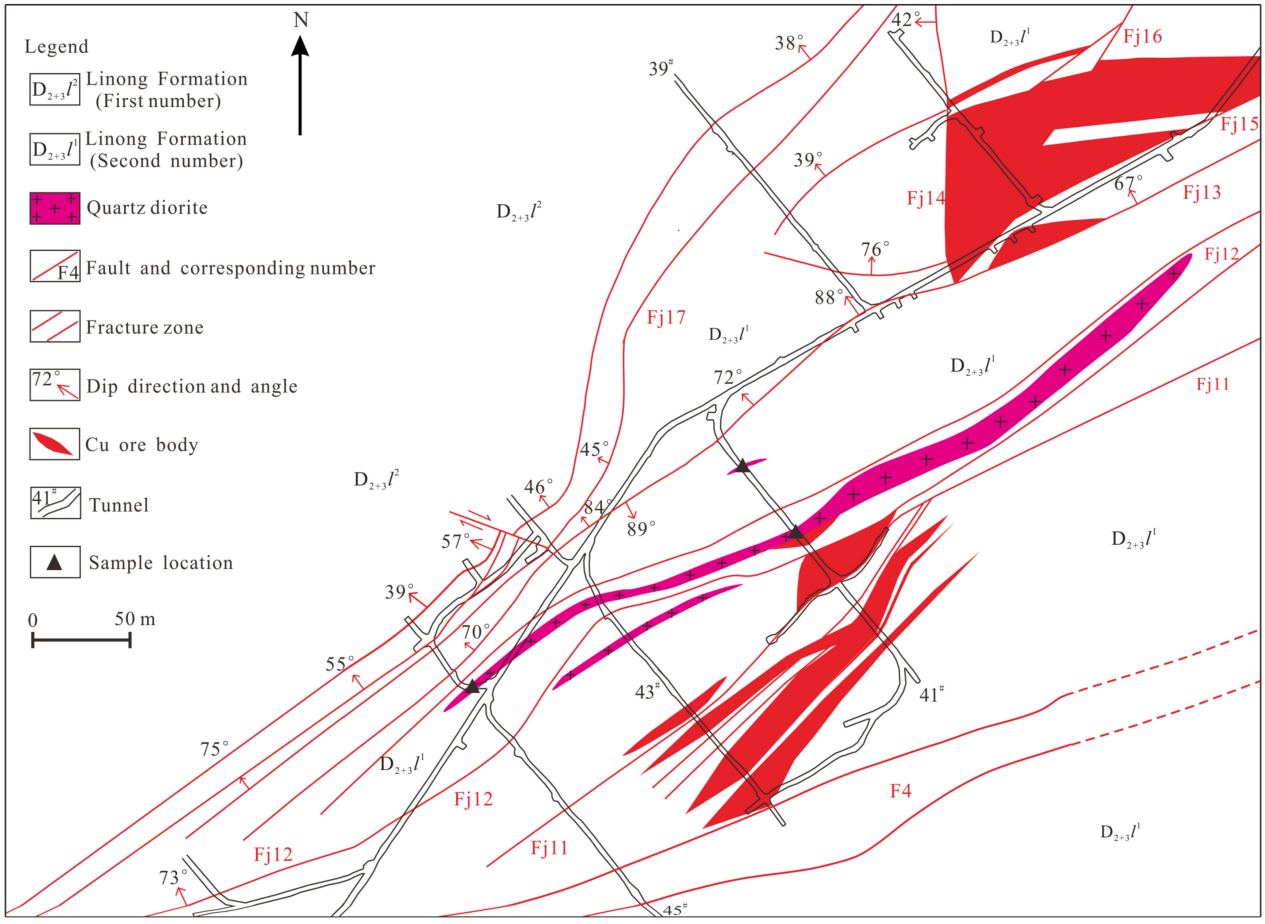

Figure 2. The sketch map of the underground tunnel 3250 m section in the Yangla Cu-W polymetallic deposit [14].

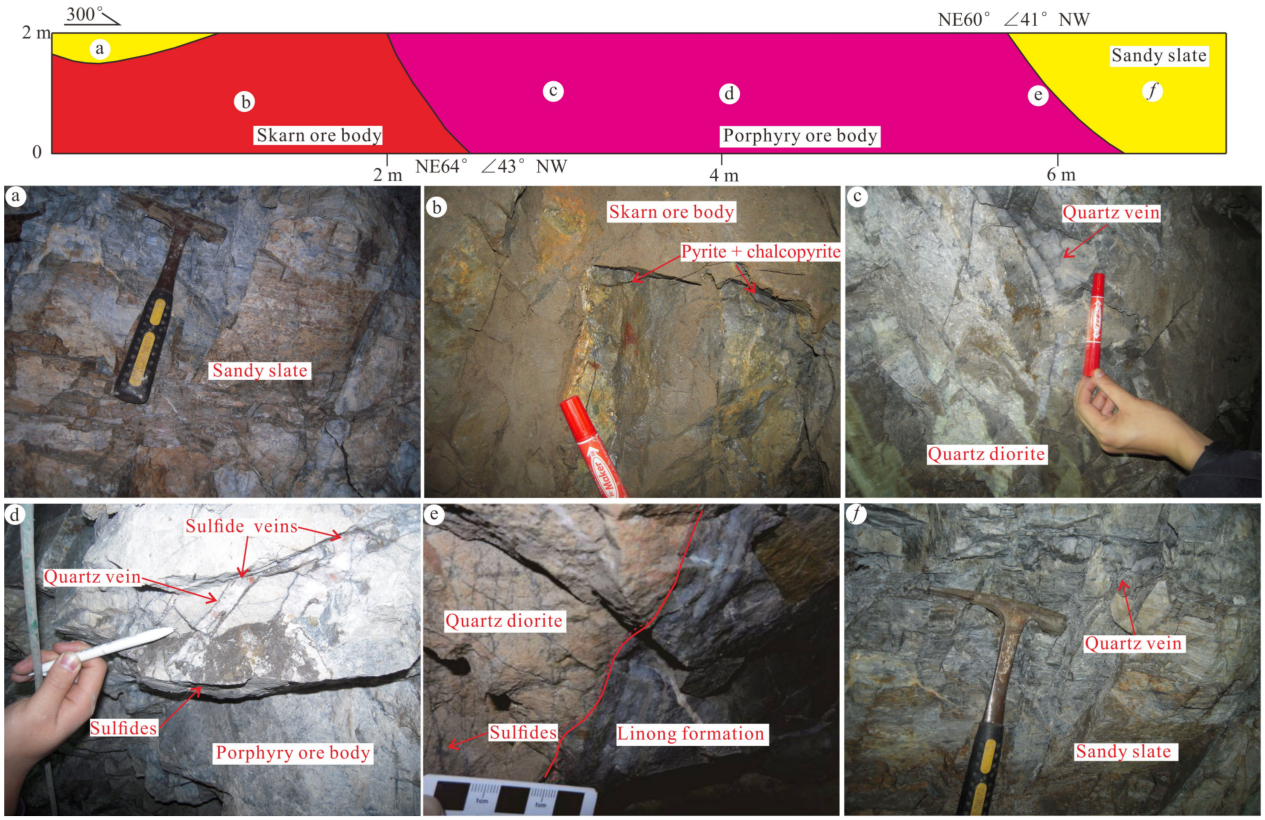

Figure 3. The sketch map of 41#-1 mining stope at underground tunnel 3250 m section in the Yangla Cu-W polymetallic deposit [13]. (**a**) The weak skarnization and silicification sandy slate; (**b**) The high-grade skarn ore body and developed disseminated pyrite and chalcopyrite; (**c**) The quartz diorite, which developed a large number of quartz veins; (**d**) The porphyry ore body, which developed vein-disseminated metal sulfides (pyrite, chalcopyrite, and sphalerite) and quartz veins; (**e**) The irregular contact line of the quartz diorite and sandy slate, which developed veins metal sulfides in the quartz diorite, and there are many quartz veins in the sandy slate of Linong Formation; (**f**) The sandy slate, which developed the later quartz veins.

Figure 4. The quartz diorite pluton and mineral features of the quartz diorite at Yangla. (**a**): Quartz diorite exposed by stop 41#-1 in the 3250 m sections of the Linong ore block. (**b**): quartz diorite exposed at stop 41#-1 in the 3250 m sections of the Linong, showing a large number of joints and fissures within the pluton, together with quartz veins. (**c**): Light-gray to grayish-white massive quartz diorite; the plagioclase phenocrysts have been altered to present grayish-white corrosion, and quartz phenocrysts are subhedral granular (Sample No. 41-1). (**d**): Light-gray to grayish-white massive quartz diorite, showing the quartz

phenocrysts that are irregular and fine-grained, together with locally developed dark-veined sulfides (Sample No. 41-3). (**e**): Light-gray to charcoal-gray massive copper-mineralized quartz diorite. Veined sulfides are developed within the quartz diorite (Sample No. 3250-41-5). (**f**): Light-gray massive quartz diorite; a small quantity of quartz-sulfide veins and disseminated sulfides are developed within the quartz diorite (Sample No. 3250-41-5). (**g**): Porphyritic quartz diorite; phenocrysts comprise corroded, embayed, irregular, and subhedral granular quartz and irregular embayed plagioclase (sericitized), and the matrix has a particulate texture and felsic nature (i.e., quartz and plagioclase) (Sample No. 41-1). (**h**): Porphyritic quartz diorite; phenocrysts comprise irregular and fine-grained quartz, irregular and embayed sericitized plagioclase, and faded biotite; the matrix has a particulate texture and felsic nature, and the phenocryst compositions are consistent with the matrix (Sample No. 41-3).

The light-gray-to-grayish-white quartz diorite samples phenocrysts are quartz (~35%), plagioclase (~30%), and biotite (~10%) (Figure 4c,d), showing subhedral-euhedral grains and corroded platy, and sheet textures. The quartz phenocrysts are mostly hexagonal and quadrangular, with smaller amounts of irregular and euhedral-subhedral crystals with corroded edges. The plagioclase phenocrysts are altered and replaced by the sericite, chlorite, and cryptocrystalline carbonate mineral. The biotite phenocrysts have been altered and replaced by sericite and other secondary minerals (Figure 4g,h). The matrix has a cryptocrystalline-microcrystalline texture and felsic nature, primarily comprising quartz, plagioclase, and biotite.

The volcanic rocks are represented by basalt (primarily composed of plagioclase, pyroxene, and hornblende), which may have formed in the Devonian to Carboniferous (at ~296 and ~362 Ma) enriched mantle source region or the cracking process of the JOB, and are confirmed to have no direct genetic relation with Cu mineralization [34]. Published U-Pb zircon ages of igneous rocks indicate that the JOB is likely to have been generated in the early Carboniferous and underwent westward-directed subduction beneath the Qamdo-Simao terrane during the Early Permian [1]. Subsequently, The JOB gradually closed and was eliminated in the Early Triassic [1]. Zircon U-Pb chronology of late diabase dikes yielded 222 Ma [35] and corresponded to the Triassic. It also has no direct genetic relation with Cu mineralization at Yangla.

3. Sampling and Analytical Methods

Three massive and medium-grained porphyritic quartz diorite samples (No. 3250-Lb41b1, 3250-Lb41b1, and 45-R4) were collected for zircon trace element and Hf isotope analyses (Figure 4a,b). Zircon grains appeared light-gray to charcoal-gray with well-defined crystal morphology, primarily presenting as a long- or short-columnar shape, with a length of 100–300 μm (Figure 5). Owing to the dark color of zircons and the weak cathodoluminescence intensity, clear magmatic oscillation zone textures (growth zones) were observed (Figure 5), indicating that these were typical magmatic zircons [36]. The Th, U, and Pb concentrations were 77–12,967 (avg. 1098 ppm), 228–12,209 (avg. 2495 ppm), and 12–467 ppm (avg.115 ppm), respectively. The Th/U ratios of quartz diorite samples were in the range of 0.15–1.48 (avg. 0.36) [14]. The U vs. Th (Figure 6a) and U vs. Pb (Figure 6b) of zircons present positive correlations and suggest they belong to the magmatic zircons [37].

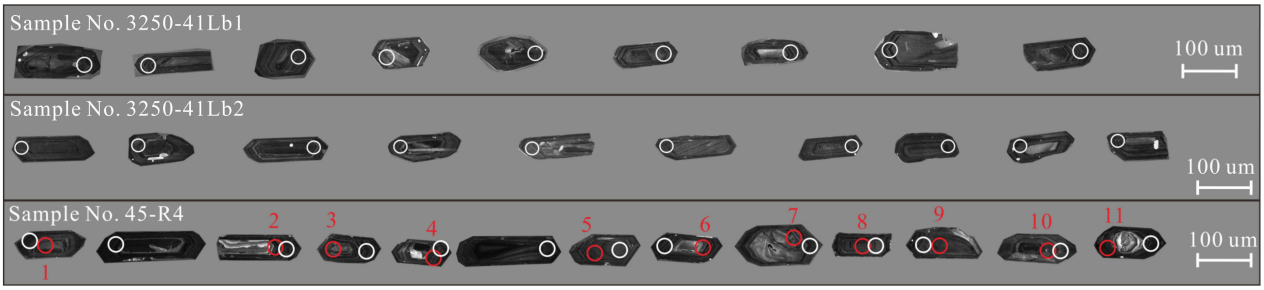

Figure 5. The CL images of zircons were analyzed for trace elements (white circles) and Hf isotopes (red circles and corresponding numbers) in quartz diorite of the Yangla Cu-W polymetallic deposit.

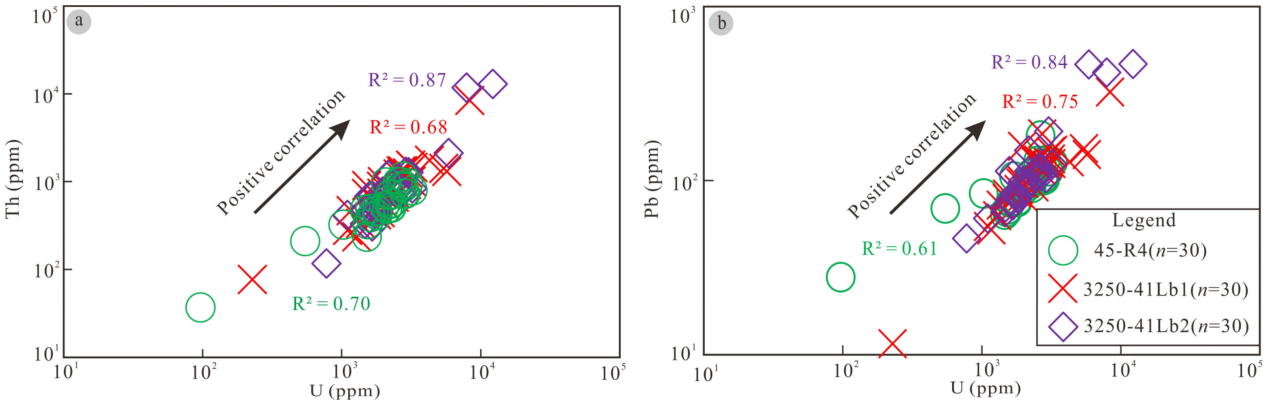

Figure 6. The zircon Th vs. U and Pb vs. U from quartz diorite in the Yangla Cu-W polymetallic deposit.

In situ zircon analyses were conducted at the State Key Laboratory of Continental Dynamics, Northwest University, Xi'an, China, using a GeoLas 2005 Laser Ablation (Agilent, Palo Alto, CA, USA) coupled with an Agilent 7500a ICP-MS. A 50 mJ/pulse (Geolas) 193 nm ArF Excimer (Lambda Physik, Göttingen, Germany) laser was used to ablate the zircons at 10 Hz. The diameter of the laser ablation spot was 32 μm. Helium was used as a carrier gas. The detailed analytical procedures used to follow those described by Yuan et al. (2010) [38]. The detection limits of LA-ICP-MS are generally lower than 0.01 ppm. Based on the zircon-reflected light images and CL images (Figure 5), we avoided inherited cores, cracks, and inclusions as far as possible. Elemental contents were calibrated by using ^{29}Si as the internal standard and NIST SRM 610 as the external standard. Raw data were processed using GLITTER (Version 4.4) [39].

In situ analysis of zircons Lu-Hf isotopic composition was carried out using laser ablation multi-collector inductively coupled plasma mass spectrometry in a laboratory of the Guangzhou Institute of Geochemistry. The ablation-spot diameter, frequency, and time were 50 μm, 8 Hz, and 30 s, respectively. The standard zircon samples (Penglai, Plešovice, and Qinghu) were used as quality control samples during the analytical process. The $^{176}Hf/^{177}Hf$ analytical results of the three standard zircons (i.e., Penglai, Plešovice, and Qinghu) were 0.282915 ± 0.000019, 0.282484 ± 0.000007, and 0.282997 ± 0.000009, respectively, which were highly consistent with the recommended values ($^{176}Hf/^{177}Hf$ = 0.282906 ± 0.00001, 0.282482 ± 0.000013, and 0.282996 ± 0.000044, respectively) for these standards [40–42]. Standard zircon $^{176}Hf/^{177}Hf$ initial values were calculated based on a decay coefficient of 1.865 × 10^{-5} Ma^{-1} [43]. The relevant parameters for calculating the Hf isotopic composition of zircon are as follows: (a) chondrite ($^{176}Hf/^{177}Hf$ = 0.282772, $^{176}Lu/^{177}Hf$ = 0.0332, and $f_{Lu/Hf}$ = 0.00); (b) depleted mantle ($^{176}Hf/^{177}Hf$ = 0.28325,$^{176}Lu/^{177}Hf$ = 0.0384, and $f_{Lu/Hf}$ = 0.16); (c) lower crust (mafic) ($^{176}Lu/^{177}Hf$ = 0.022 and $f_{Lu/Hf}$ = −0.34); (d) upper crust (felsic) ($^{176}Lu/^{177}Hf$ = 0.0093 and $f_{Lu/Hf}$ = −0.72); (e) average crust ($^{176}Lu/^{177}Hf$ = 0.015 and $f_{Lu/Hf}$ = −0.55) [44–46].

4. Results

4.1. Zircon Trace Elements Compositions

The trace element compositions of zircons from samples 45-R4, 3250-42Lb1, and 3250-41Lb2 for the quartz diorite are listed in Table 1 and Supplementary Table S1. Moreover, we cited zircons trace element compositions of Yangla dioritic enclaves, granodiorite, and quartz monzonite porphyry plutons, and the details data have been described by reference [3]. Chondrite-normalized REE patterns of most zircons are characterized by left-inclined (depletion of LREE and enrichment of HREE), with positive Ce anomalies (δCe) and negative Eu anomalies (δEu) (Figure 7), which is similar to typical magmatic zircon REE patterns [47]. In addition, we have noticed that a small number of zircons have positive Eu anomalies (δEu > 1.0), which may be that the zircons were affected by crystallization fractionation of mineral phase (i.e., plagioclase, apatite, and titanite) [23], oxidation conditions of the melt [48,49], and (or) later hydrothermal alteration [50]. Zircons in three quartz diorite samples yield a relatively wide range of ∑REE between 150 and 6218 ppm (avg. 1316 ppm), similar δCe values in a range between 1.0 and 141.31 (average = 8.48), and δEu values of 0.24–3.03 (avg. 0.90). The variations of ∑REE may be attributed to (i) the coeval fractional crystallization of accessory minerals (i.e., apatite) [51] and (ii) the later fluid metasomatism or involved [48,52]. For zircons of two dioritic enclave samples, the ∑REE content ranges from 321 to 917 ppm (avg. 559 ppm), with δCe of 1.06–89.74 (avg. 19.53) and δEu of 0.08–2.31 (avg. 0.53) [3]. For zircons of three GR samples, the ∑REE content ranges from 353 to 1716 ppm (avg. 660 ppm), with δCe of 2.0–139 (avg. 16) and δEu of 0.19–1.70 (avg. 0.51) [3]. For zircons of two quartz monzonite porphyry samples, the ∑REE content ranges from 515 to 1300 ppm (avg. 801 ppm), with δCe of 1.12–49.95 (avg. 8.37) and δEu of 0.12–0.94 (avg. 0.41) [3].

Table 1. LA-ICP-MS analytical results of zircon trace elements (ppm), Ti-in-zircon temperatures (T_{Ti}/°C), and oxygen fugacity parameters (ΔFMQ) in the Yangla quartz diorite.

No.	Ti	Nb	La	Ce	Pr	Nd	Sm	Eu	Gd	Tb	Dy	Ho	Er	Tm	Yb	Lu	Y	Hf	Ta	Pb	Th	U	ΣREE	δEu	δCe	T_{Ti}/°C	ΔFMQ
Sample No. 45-R4																											
Min.	1.44	3.11	0.01	5.33	0.01	0.35	1.61	0.37	12.41	4.61	53.80	20.94	104.60	24.12	231.96	48.79	584	7667	1.83	64	210	547	519	0.24	1.12	616	−2.54
Max	19.61	19.49	35.91	99.56	13.13	70.31	52.35	19.91	159.56	38.45	302.07	79.13	310.28	70.22	671.96	146.01	2277	10,400	5.95	181	1147	3249	1663	1.52	112.11	853	2.26
Avg.	6.61	6.50	2.43	16.24	1.34	9.53	11.63	5.15	39.73	12.24	131.19	47.10	212.36	48.31	450.90	95.87	1319	8941	3.89	98	620	2144	1084	0.76	12.41	725	−1.42
Sample No. 3250-41Lb1																											
Min.	1.24	1.44	0.09	5.14	0.07	0.75	1.63	0.31	9.70	4.15	34.39	8.79	27.09	4.39	32.85	5.89	239	6000	0.51	12	77	228	150	0.24	1.01	606	−2.45
Max	26.32	23.39	81.74	176.43	22.61	109.39	38.19	51.54	122.22	33.32	353.63	134.95	604.98	133.76	1174.65	234.10	3593	9834	10.28	322	8398	8358	2898	3.03	20.09	887	3.14
Avg.	10.08	7.21	9.57	38.17	4.14	23.38	16.25	10.54	51.14	16.13	170.57	59.37	257.06	57.40	518.59	107.53	1583	8319	4.34	115	1160	2646	1340	0.99	3.05	761	−0.66
Sample No. 3250-41Lb2																											
Min.	1.51	2.19	0.01	4.06	0.04	0.50	2.72	0.60	15.34	5.71	70.05	26.34	108.91	25.30	239.91	54.07	690	5058	1.95	46	117	776	617	0.27	1.23	620	−2.49
Max	77.70	65.26	14.94	255.53	11.78	94.32	235.78	66.68	717.38	168.19	1120.49	282.38	1235.61	274.17	2404.16	492.56	7529	9156	13.39	467	12,967	12,209	6218	2.58	141.31	1036	0.26
Avg.	10.45	9.47	2.43	29.36	2.13	16.31	22.24	11.49	72.85	21.08	205.51	69.05	294.53	65.37	587.53	122.81	1851	8110	4.64	133	1514	2695	1523	0.97	10.00	748	−1.20

Note: The Min, Max, and Avg. values correspond to a single quartz diorite sample. The detailed trace element concentrations are shown in Supplementary Table S1.

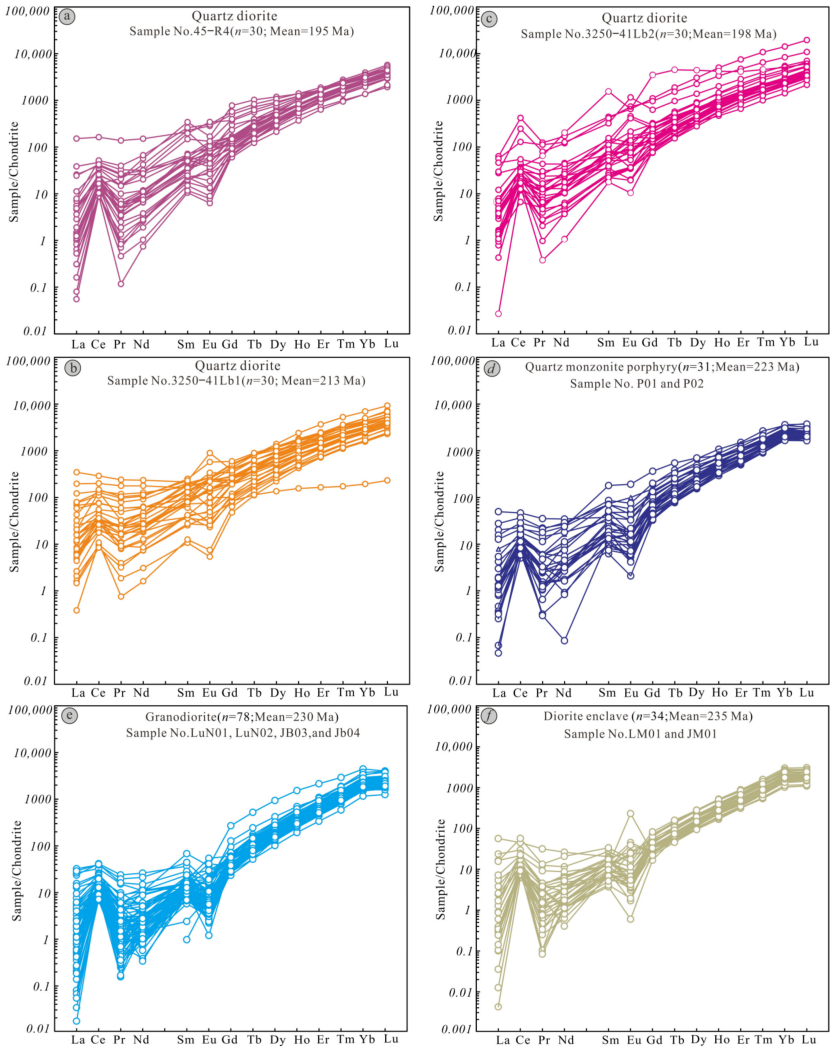

Figure 7. Plots of chondrite-normalized REE contents in zircons from Yangla granitoid plutons. The zircons data of granodiorite, diorite enclave, and quartz monzonite porphyry were sourced the Ref. [3]. Normalization values for chondrite after Ref. [53]. (**a**–**c**) chondrite-normalized REE patterns in zircon grains from Yangla quartz diorite; (**d**) chondrite-normalized REE patterns in zircon grains from Yangla quartz monzonite porphyry; (**e**) chondrite-normalized REE patterns in zircon grains from Yangla granodiorite; (**f**) chondrite-normalized REE patterns in zircon grains from Yangla diorite enclave.

4.2. Hf Isotopic Compositions of Quartz Diorite

Zircon $^{176}Yb/^{177}Hf$ and $^{176}Lu/^{177}Hf$ ratios of the quartz diorite ranged from 0.024001 to 0.050774 (avg. 0.037560) and 0.001881 to 0.001446 (avg. 0.001194), respectively. The ratios of $^{176}Lu/^{177}Hf$ were relatively similar, and all ratios were less than 0.002 (Table 2), suggesting that there was essentially no accumulation of radioactive Hf after the formation of the zircon crystals, and the initial $^{176}Lu/^{177}Hf$ values can be represented by the $^{176}Lu/^{177}Hf$ ratios of the zircon crystals [5]. The $(^{176}Hf/^{177}Hf)_t$, $\varepsilon_{Hf}(0)$, $\varepsilon_{Hf}(t)$, t_{DM}, and t^{C}_{DM} were 0.28233–0.282470 (avg. 0.282403), −15.39 to −10.58 (avg. −12.90), −11.28 to −6.40 (avg. −8.77), 1099–1299 Ma (avg. 1200 Ma), and 1643–1950 Ma (avg. 1972 Ma), respectively. The $f_{Lu/Hf}$ was −0.97 to −0.96, with an average of −0.96, significantly lower than that of the mafic lower crust ($f_{Lu/Hf}$ = −0.34) [54], sialic upper crust ($f_{Lu/Hf}$ = −0.72) [55], average crust ($f_{Lu/Hf}$ = −0.55) [46], depleted mantle ($f_{Lu/Hf}$ = +0.16) [45], and chondrites ($f_{Lu/Hf}$ = 0.00) [56].

Table 2. Zircon Hf isotopic compositions of quartz diorite, granodiorite, quartz monzonite porphyry, and dioritic enclave in the Yangla Cu-W polymetallic deposit.

Intrusions Type	No.	Age/Ma	$^{176}Yb/^{177}Hf$	$^{176}Lu/^{177}Hf$	$^{176}Hf/^{177}Hf$	2σm	$(^{176}Hf/^{177}Hf)_t$	$\varepsilon_{Hf}(0)$	$\varepsilon_{Hf}(t)$	t_{DM}(Ma)	t^{C}_{DM}(Ma)	$f_{Lu/Hf}$	Reference
Quartz diorite (45-R4; N = 11)	1	195	0.047665	0.001408	0.282383	0.000029	0.282378	−13.77	−9.66	1241	1849	−0.96	This paper
	2	195	0.044598	0.001346	0.282420	0.000033	0.282415	−12.46	−8.35	1187	1766	−0.96	
	3	195	0.050774	0.001446	0.282403	0.000030	0.282398	−13.03	−8.95	1213	1803	−0.96	
	4	195	0.027950	0.000981	0.282404	0.000029	0.282400	−13.03	−8.88	1198	1799	−0.97	
	5	195	0.041369	0.001387	0.282400	0.000030	0.282395	−13.17	−9.05	1217	1812	-0.96	
	6	195	0.039769	0.001327	0.282421	0.000023	0.282417	−12.40	−8.28	1184	1762	−0.96	
	7	195	0.039664	0.001204	0.282385	0.000035	0.282381	−13.67	−9.55	1231	1842	−0.96	
	8	195	0.029164	0.001035	0.282410	0.000027	0.282406	−12.81	−8.66	1191	1785	−0.97	
	9	195	0.026465	0.000911	0.282473	0.000029	0.282470	−10.58	−6.40	1099	1643	−0.97	
	10	195	0.024001	0.000881	0.282446	0.000025	0.282442	−11.54	−7.39	1136	1704	−0.97	
	11	195	0.041744	0.001207	0.282337	0.000034	0.282332	−15.39	−11.28	1299	1950	−0.96	
	Min.	195	0.024001	0.000881	0.282337	0.000023	0.282332	−15.39	−11.28	1099	1643	−0.97	
	Max.	195	0.050774	0.001446	0.282473	0.000035	0.282470	−10.58	−6.40	1299	1950	−0.96	
	Avg.	195	0.037560	0.001194	0.282407	0.000029	0.282403	−12.90	−8.77	1200	1792	−0.96	
Quartz monzonite porphyry (N = 31)	Min.	188	0.019956	0.000844	0.282401	0.000021	0.282396	−13.12	−8.18	894	1268	−0.97	[3]
	Max.	267	0.051689	0.002051	0.282622	0.000047	0.282617	−5.31	0.37	1207	1785	−0.94	
	Avg.	230	0.031792	0.001297	0.282513	0.000027	0.282508	−9.15	−4.29	1054	1536	−0.96	
Granodiorite (N = 192)	Min.	213	0.017773	0.000672	0.282391	0.000009	0.282387	−13.47	−8.50	767	1082	−0.98	[2–5]
	Max.	239	0.092584	0.002346	0.282713	0.000038	0.282708	−2.09	2.86	1217	1805	−0.93	
	Avg.	230	0.036373	0.001163	0.282595	0.000021	0.282590	−6.26	−1.43	934	1337	−0.97	
Dioritic enclaves (N = 38)	Min.	229	0.016020	0.000735	0.282479	0.000019	0.282475	−10.37	−5.30	806	1147	−0.98	[3]
	Max.	241	0.040573	0.001727	0.282684	0.000027	0.282680	−3.11	1.87	1089	1606	−0.95	
	Avg.	235	0.025544	0.001159	0.282587	0.000023	0.282582	−6.53	−1.54	946	1366	−0.97	

4.3. Hf Isotopic Compositions of Other Granitoid Plutons

The Hf isotopic compositions values of five granodiorites (Beiwu, Jiangbian, Linong, Lunong, and Tongjige), a dioritic enclave, and a quartz monzonite porphyry were systematically obtained to analyze and discuss the origin, evolution, and geodynamic setting of magma in the YCWPD (Table 2). The details data of Yangla dioritic enclaves, GR, and quartz monzonite porphyry plutons have been described by the references [2–5].

The granodiorite zircons had $^{176}Yb/^{177}Hf$ and $^{176}Lu/^{177}Hf$ ratios of 0.017773–0.092584 (avg. 0.036373) and 0.000672–0.002346 (avg. 0.001163), respectively. The $(^{176}Hf/^{177}Hf)_t$, $\varepsilon_{Hf}(0)$, $\varepsilon_{Hf}(t)$, t_{DM}, and t^{C}_{DM} were 0.282387–0.282708 (avg. 0.282590), −13.47 to −2.09 (avg. −6.26), −8.50 to 2.86 (avg. −1.43), 767–1217 Ma (avg. 934 Ma), and 1082–1805 Ma (avg. 1337 Ma), respectively. The $f_{Lu/Hf}$ was −0.98 to −0.93, with an average of −0.97 [2–5].

Dioritic enclave zircons had $^{176}Yb/^{177}Hf$ and $^{176}Lu/^{177}Hf$ ratios of 0.016020–0.040573 (avg. 0.025544) and 0.000735–0.001727 (avg. 0.001159), respectively. The $(^{176}Hf/^{177}Hf)_t$, $\varepsilon Hf(0)$, $\varepsilon_{Hf}(t)$, t_{DM}, and t^{C}_{DM} were 0.282475–0.282680 (avg. 0.282582), −10.37 to −3.11 (avg. −6.53), −5.30 to 1.87 (avg. −1.54), 806–1089 Ma (avg. 946 Ma), and 1147–1606 Ma (avg. 1366 Ma), respectively. fLu/Hf was -0.98 to -0.95, with an average of −0.97 [3].

Quartz monzonite porphyry zircons had $^{176}Yb/^{177}Hf$ and $^{176}Lu/^{177}Hf$ ratios of 0.019956–0.051689 (avg. 0.031792) and 0.000844–0.002051 (avg. 0.001297), respectively. The $(^{176}Hf/^{177}Hf)_t$, $\varepsilon_{Hf}(0)$, $\varepsilon_{Hf}(t)$, t^{DM}, and t^{C}_{DM} were 0.282396–0.282617 (avg. 0.282508), −13.12 to −5.31 (avg. −9.15), −8.18 to 0.37 (avg. −4.29), 894–1207 Ma (avg. 1054 Ma), and 1268–1785 Ma (avg. 1536 Ma), respectively. The fLu/Hf was −0.97 to −0.94, with an average of −0.96 [3].

4.4. Comparison of Yangla Granitoid Plutons

The chronology and Hf isotopic geochemistry of the granodiorite, dioritic enclaves, quartz monzonite porphyry, and quartz diorite were analyzed and compared to facilitate the discussion and constraint of the magma origin, evolution, and geodynamic tectonic setting in the YCWPD.

4.4.1. Geochronology

The emplacement ages of the granodiorite are mainly concentrated between 208 and 246 Ma (N = 28; avg. 230 Ma), suggesting that the Yangla granodiorite pluton was formed in the Triassic (~230 Ma). The crystallization ages of the dioritic enclaves within the granodiorite are 232 and 238 Ma (avg. 235 Ma) [3], also indicating formation in the Triassic (~235 Ma). The whole-rock Rb-Sr age of the quartz monzonite porphyry is 202 Ma [33], whereas the zircon U-Pb crystallization ages are 232 Ma and 234 Ma, giving an overall average of 223 Ma [3], suggesting that the quartz monzonite porphyry also formed in the Triassic, and slightly later than the granodiorite and dioritic enclaves. The emplacement ages of the quartz diorite are 195, 198, and 213 Ma (avg. 202 Ma), indicating that the quartz diorite formed in the Late Triassic to Early Jurassic, slightly later than the above-mentioned Yangla granitoid plutons [14]. Therefore, the emplacement ages of the granitoid plutons show an obvious decrease from dioritic enclaves (~232 Ma), through granodiorite (~208 Ma), and to quartz monzonite porphyry (~202 Ma) and quartz diorite (~195 Ma) in the Yangla mining district (Table 3, Figure 8).

Table 3. The integration of published geochronological data for various granitic plutons in Yangla Cu-W polymetallic deposit.

Intrusions Type	Minerals/Methods	Age/Ma	References
Quartz diorite	Zircon/U-Pb	195.3 ± 6.4, 198.40 ± 8.6, and 213 ± 15	[14]
Quartz monzonite porphyry	Zircon/U-Pb	232 ± 1.1 and 234.0 ± 1.2.	[3]
	Whole-rock/Rb-Sr	202	[33]
Beiwu granodiorite	Zircon/U-Pb	213.6 ± 6.9 and 233.9 ± 1.4	[2,4]
Jiangbian granodiorite	Zircon/U-Pb	227.9 ± 5.1, 232.0 ± 0.5, 232.0 ± 0.9, 238.0 ± 0.5, 208.09 ± 0.46, 215.7 ± 0.63, 221.28 ± 1.0, 220.3 ± 1.3, and 214.7 ± 0.56.	[3,4,6]
Linong granodiorite	Zircon/U-Pb	239.0 ± 5.7, 229.6 ± 4.4, 233.1 ± 1.4, 234.1 ± 1.2, 235.6 ± 1.2, 232.0 ± 0.9, 233.0 ± 0.9Ma, 224 ± 0.7, 232 ± 1.1, and 234 ± 1.2	[2–4,6]
Lunong granodiorite	Zircon/U-Pb	238.1 ± 5.3, 231.0 ± 1.6, 230 ± 1.9, and 234 ± 0.8.	[2–4]
Tongjige granodiorite	Zircon/U-Pb	246.1 ± 3.1, 225.6 ± 1.3, and 226.1 ± 3.3	[5,35]
Dioritic enclaves	Zircon/U-Pb	232 ± 0.9 and 238 ± 0.5.	[3]

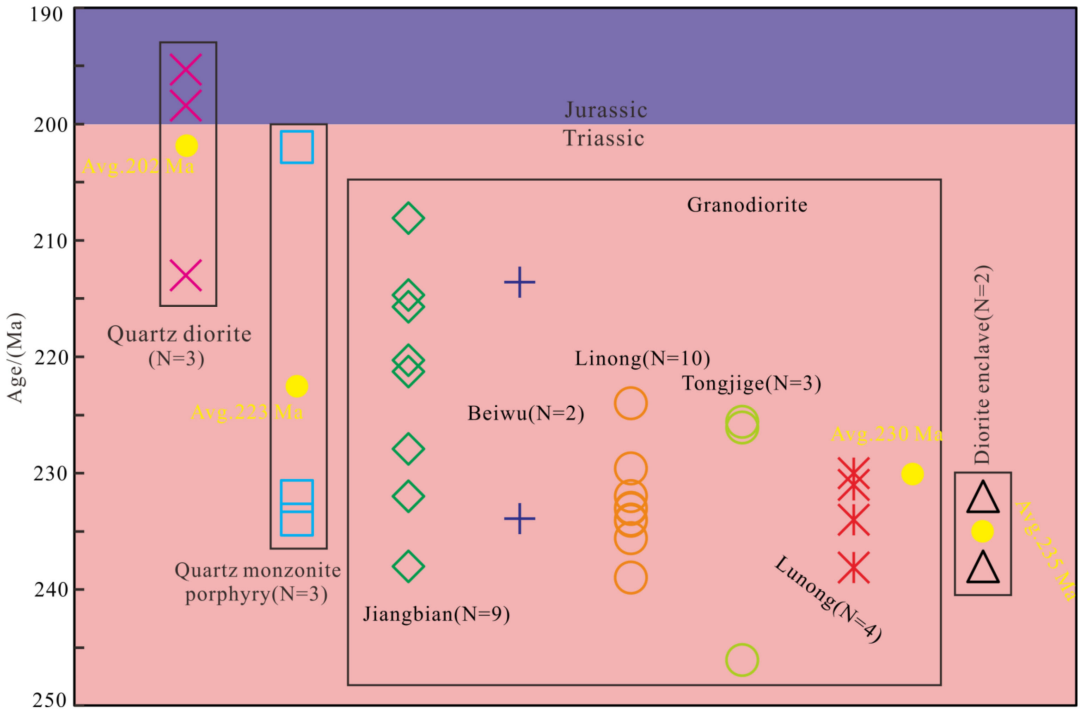

Figure 8. The integration of published geochronological data for various granitic plutons at Yangla Cu-W polymetallic deposit. The signs (i.e., circles, crosses, triangles, rhombus, and squares) represents the emplacement ages of different granitoid plutons.

4.4.2. Hf Isotopic Geochemistry

The $^{176}Yb/^{177}Hf$ ratios of the DE, GR, quartz monzonite porphyry and quartz diorite are basically consistent with each other. The average values of $^{176}Yb/^{177}Hf$ moving from the DE to the quartz diorite present a difference of only 0.012016, with a small variation range, and there is a consistent range in the $^{176}Yb/^{177}Hf$ ratio distribution diagram (Table 2; Figure 9a). The $^{176}Lu/^{177}Hf$ ratios of dioritic enclaves, granodiorite, quartz monzonite porphyry, and quartz diorite also generally show a smaller variation. The average values of $^{176}Lu/^{177}Hf$ moving from the dioritic enclaves to the quartz diorite present a difference of only 0.000138, with a small variation range, and there is a consistent range in the $^{176}Yb/^{177}Hf$ ratio distribution diagram (Table 2; Figure 9b). The $^{176}Hf/^{177}Hf$ and

($^{176}Hf/^{177}Hf)_t$ ratios of these granitoids generally show that dioritic enclaves are roughly equal to GR, greater than quartz monzonite porphyry, and followed by the quartz diorite (Table 2; Figure 9c,d). The $\varepsilon_{Hf}(0)$ and $\varepsilon_{Hf}(t)$ values of these granitoids generally show that the dioritic enclaves are roughly equal to granodiorite, greater than quartz monzonite porphyry, and followed by the quartz diorite (Table 2; Figure 10a,b). The mean difference of $\varepsilon_{Hf}(0)$ and $\varepsilon_{Hf}(t)$ between quartz diorite and that of granodiorite are 6.64 and 7.34, respectively. The t_{DM} and t^{C}_{DM} values generally show that dioritic enclaves are roughly equal to granodiorite, lower than quartz monzonite porphyry and quartz diorite (Table 2; Figure 10c,d). The mean difference of t_{DM} and t^{C}_{DM} between quartz diorite and that of granodiorite is 266 Ma and 455 Ma, respectively.

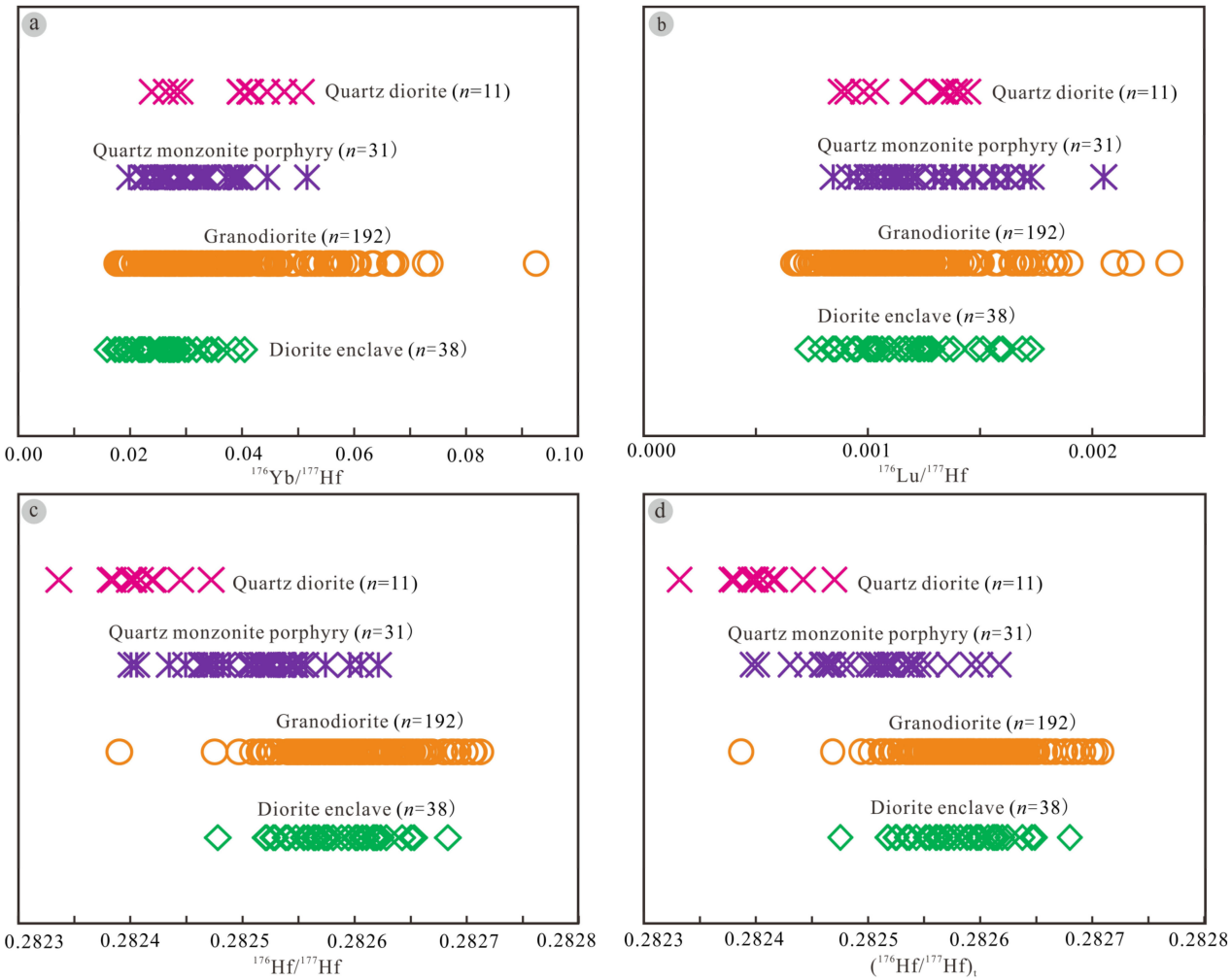

Figure 9. The diagram of variations (**a**) $^{176}Yb/^{177}Hf$, (**b**) $^{176}Lu/^{177}Hf$, (**c**) $^{176}Hf/^{177}Hf$, and (**d**) $(^{176}Hf/^{177}Hf)_t$ from zircons in the Yangla granitoid intrusions.

In summary, the quartz diorite, granodiorite, dioritic enclaves, and quartz monzonite porphyry have similar characteristics in terms of their $^{176}Yb/^{177}Hf$ and $^{176}Lu/^{177}Hf$ ratios but show evident differences in their $^{176}Hf/^{177}Hf$, $\varepsilon_{Hf}(t)$, t_{DM}, and t^{C}_{DM} values. This may be related to the differences in emplacement age, magma source, and evolutionary processes of each granitoid pluton. The reasons for the differences in the Lu-Hf isotopic system of the Yangla granitoids will be discussed in the following Section 5.

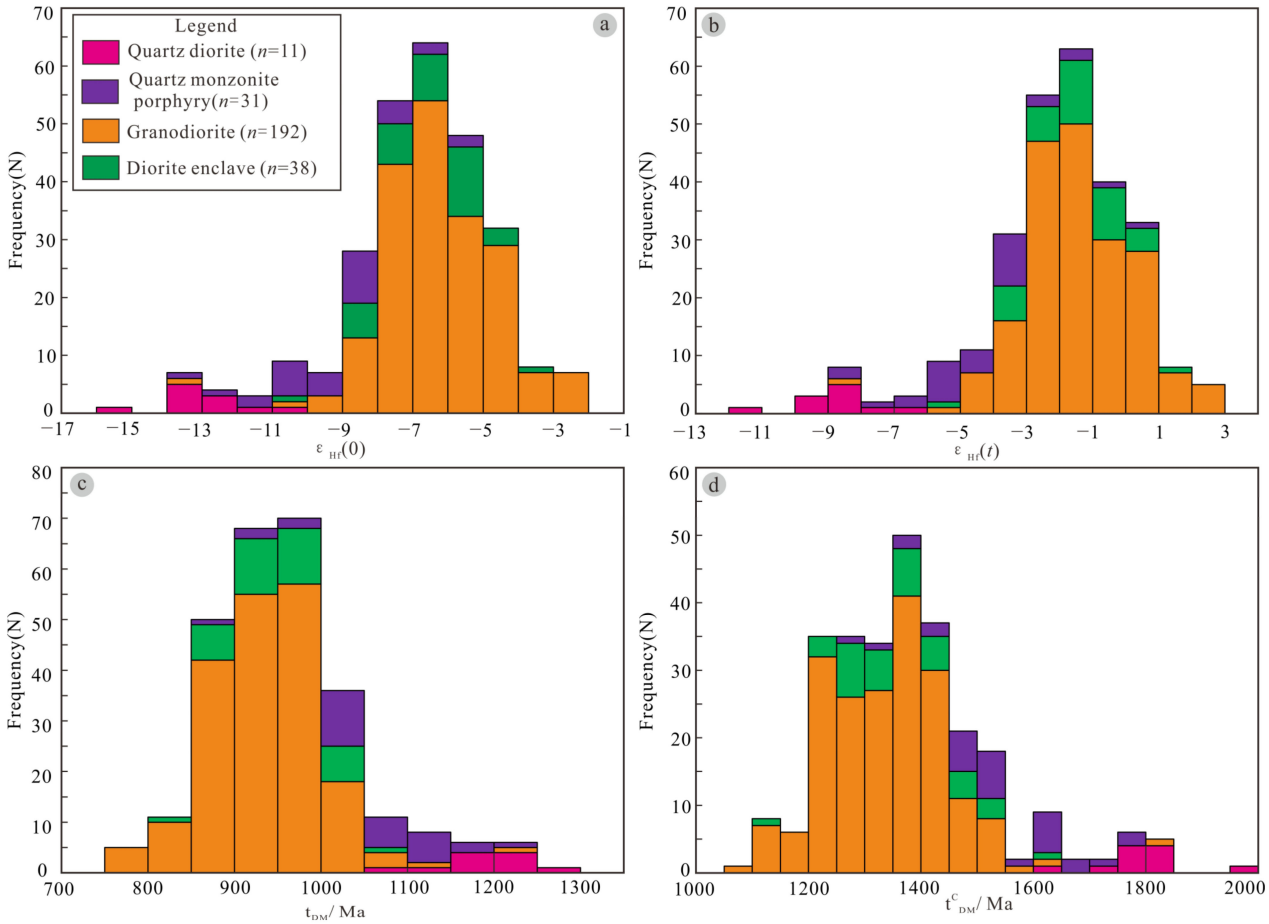

Figure 10. The histogram of (**a**) $\varepsilon_{Hf}(0)$, (**b**) $\varepsilon_{Hf}(t)$, (**c**) t_{DM}, and (**d**) t^{C}_{DM} for zircons from Yangla granitoid intrusions.

4.5. Crystallization Temperature

Zircon is regarded as a preferred accessory mineral for estimating magma formation temperature due to its high stability and early crystallization in granitic magmatic systems [57–59]. Ferry and Watson (2007) [60] have suggested that the $ZrSiO_4$, $ZrTiO_4$, and $TiSiO_4$ are the independent variation phases, and the Ti mainly replaces the Si, and the replacement equation is $ZrSiO_4 + TiO_2 \leftrightarrow ZrTiO_4 + SiO_2$ or $TiO_2 + SiO_2 \leftrightarrow TiSiO_4$ in zircons. They have revised and proposed a new calculation equation of zircons crystallization temperature as follows:

$$\lg(\mathrm{Ti})\mathrm{zircon} = (5.711 \pm 0.072) - (4800 \pm 86)/\mathrm{T(k)} + \lg(\alpha TiO_2) - \lg(\alpha SiO_2) \quad (1)$$

The lg(Ti)zircon represents the concentrations of Ti in zircons (ppm). It is generally assumed that αSiO_2 and αTiO_2 are equal to 1 if quartz and rutile are present in the magmatic system, respectively. In particular, if the magma system does not contain rutile but contains other Ti-containing minerals (i.e., titanite and ilmenite), the αTiO_2 generally varies between 0.5 and 1.0 [61]. The Yangla granodiorite intrusions are SiO_2 saturated, and coexisting Ti-bearing phases (ilmenite) indicate αTiO_2 is not low [3]. The αTiO_2 has been assumed to be 0.70 in the Yangla granodiorite, and this article will continue to cite this hypothetical result [3]. The calculation reveals that the zircons in three quartz diorites have a model temperature range of 606–1036 °C, with average crystallization temperatures of approximately 745 °C (Table 1 and Figure 11a), which are notable that the crystallization temperatures of quartz diorite are slightly higher than those of most granodiorite (avg. 661 °C, n = 72), dioritic enclaves (avg. 634 °C, n = 31), and quartz monzonite porphyry (avg. 651 °C, n = 24) zircons samples (Table 1 and Figure 11a) [3]. Therefore, we preliminarily believe

that the magma crystallization temperature gradually increased from early to late stages, corresponding to the dioritic enclaves → granodiorite → quartz monzonite porphyry → quartz diorite in the Yangla mining district.

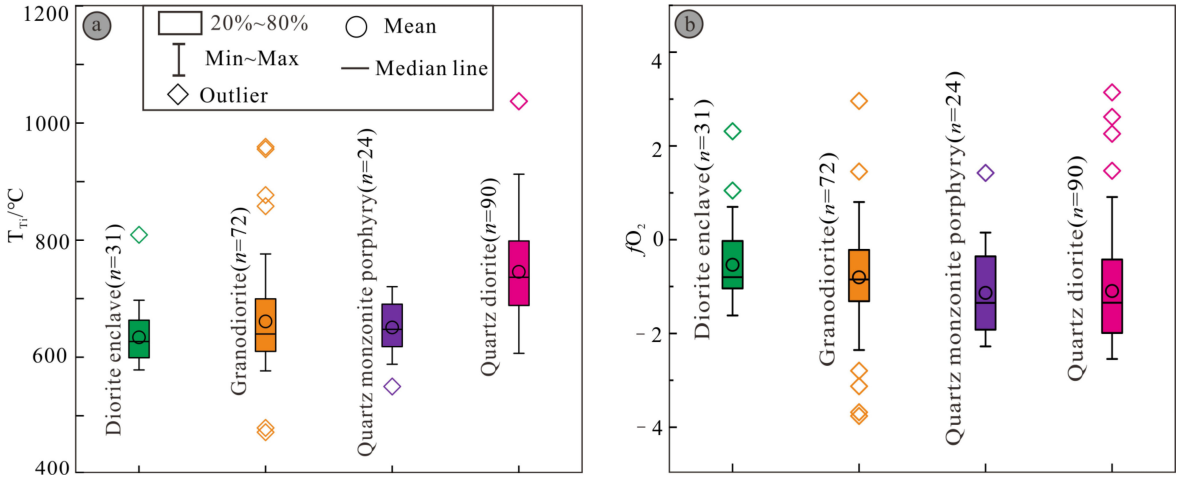

Figure 11. The zircons crystal temperature and oxygen fugacity diagram of Yangla granitoid plutons. (**a**) comparative box plots for the zircons crystal temperature and (**b**) oxygen fugacity.

4.6. Oxygen Fugacity

Zircon rare earth elements (REEs) oxy-barometers have been widely used to calculate magma oxygen fugacity, and there are mainly seven types of commonly used zircon REEs oxy-barometer [62], such as $(Ce^{4+}/Ce^{3+})_{Zircon}$ [19], $(Ce/Ce^*)_D$, $(Eu/Eu^*)_D$, $(Ce/Ce^*)_{CHUR}$ [63], $(Ce/Ce^*)_C$ [23,25], Ce/Nd ratios [64], and $(X^{melt}_{Ce^{4+}}/X^{melt}_{Ce^{3+}})_{Zircon}$ [65]. The $(Ce^{4+}/Ce^{3+})_{Zircon}$ oxy-barometers will be largely affected by an obvious deviation to the lattice strain model, and only when $\delta K < 3.0$ can $(Ce^{4+}/Ce^{3+})_{Zircon}$ yield a robust semi-quantitative oxygen fugacity [62]. The $(Ce/Ce^*)_D$, $(Ce/Ce^*)_{CHUR}$, and Ce/Nd oxy-barometers largely depend on the accurate La concentrations in zircons [57,62]. However, when zircons with La $\leq$ 0.1 ppm (clean zircons) are considered to truly reflect the REE composition of zircon, free from excess nonlattice bound REEs contributed by inclusions, and accurate oxygen fugacity can be obtained [62]. The La concentrations of zircons in Yangla quartz diorite, granodiorite, dioritic enclaves, and quartz monzonite porphyry are generally greater than 0.1 ppm, indicating that the above-mentioned oxy-barometers may not reflect accurate oxygen fugacity. The $(X^{melt}_{Ce^{4+}}/X^{melt}_{Ce^{3+}})_{Zircon}$ oxy-barometer does not rely on the accurate measurement of La content in zircons or limited deviation from the lattice strain model. However, the $(X^{melt}_{Ce^{4+}}/X^{melt}_{Ce^{3+}})_{Zircon}$ oxy-barometer still requires accurate measurement of H_2Owt%, temperature (T), and $D^{zircon/whole\ rock}_{Ce^{4+}}$ in the melt [62]. The estimates of H_2Owt% values have a greater impact on final oxygen fugacity, and it is generally difficult to obtain an accurate water content of the magma at the time of zircon crystallization [62]. The $(Ce/Ce^*)_C$ calculation formula is as follows:

$$(Ce/Ce^*)_C = Ce_N/[(Nd_N)^2/Sm_N] \quad (2)$$

This formulation is much more robust than the conventional method as it does not require the accurate determination of either La or Pr [23]. However, when combined with Equation (3) to calculate the oxygen fugacity and the calculated results are dominated by negative values and significantly lower than those of most ore-bearing intrusions (i.e., Relin, Tongchanggou, Disug, and Pulang in Sanjiang polymetallic metallogenic belt of Southwest China, and Dexing in Jiangnan orogen belt of southern China) [66,67].

This calculation formula is not suitable for the estimation of oxygen fugacity in Yangla granitoids plutons.

$$\ln(Ce/Ce^*) = (0.1156 \pm 0.0050) \times \ln fo_2 + (13.860 \pm 708)/T - (6.125 \pm 0.48) \quad (3)$$

Therefore, this study mainly adopts the zircon oxy-barometer independent of the melt composition proposed by Loucks et al. (2020) [68], which can well avoid the main problems involved in the above-mentioned oxy-barometers. The calculation formula is as follows:

$$\log fO_{2(\text{sample})} - \log fO_{2(\text{FMQ})} = \Delta\text{FMQ} = 3.99_8(\pm 0.12_4) \times \log\left[\frac{Ce}{\sqrt{U_i \times Ti}}\right] + 2.28_4(\pm 0.10_1) \quad (4)$$

$$U_i = U_{\text{zircon}} \times e^{1.98173 \times 10^{-4} \times t} \quad (5)$$

The Ce and Ti represent the concentrations in zircons. The t represents the age of zircon crystallization (Ma). The calculation reveals that the zircons in three quartz diorites have a ΔFMQ range of −2.54–+3.14, with an average of −1.09. Correspondingly, log$fO_{2(\text{quartz diorites})}$ ranges from FMQ – 2.54 to FMQ +3.14, with an average of FMQ −1.09. The oxygen fugacity of granodiorite, dioritic enclaves, and quartz monzonite porphyry zircons samples mainly concentrated in FMQ −3.76 to FMQ + 2.96, FMQ −1.60 to FMQ +2.31, FMQ −2.27 to FMQ +1.43, respectively. The oxygen fugacity of quartz diorite is slightly lower than those of most granodiorite (ΔFMQ = −3.76 to 2.96, avg. −0.80, n = 72), dioritic enclaves (ΔFMQ = −1.60 to 2.31, avg. −0.52, n = 31), and quartz monzonite porphyry (ΔFMQ = −2.27 to 1.43, avg. −1.10, n = 24) samples (Table 1 and Figure 11b), indicating that the oxygen fugacity of granitic magma gradually decreased during the magma evolution from early to a late stage in the Yangla mining district. This evolving pattern can be further supported by the varied Ce/Nd ratios of Yangla granitoid zircons. The Ce/Nd ratios of zircons show a slight decrease from dioritic enclave and granodiorite, through quartz monzonite porphyry, and to quartz diorite (Figure 12a), which indicates that they are relatively reduced compared to the dioritic enclave and granodiorite in the Yangla mining district.

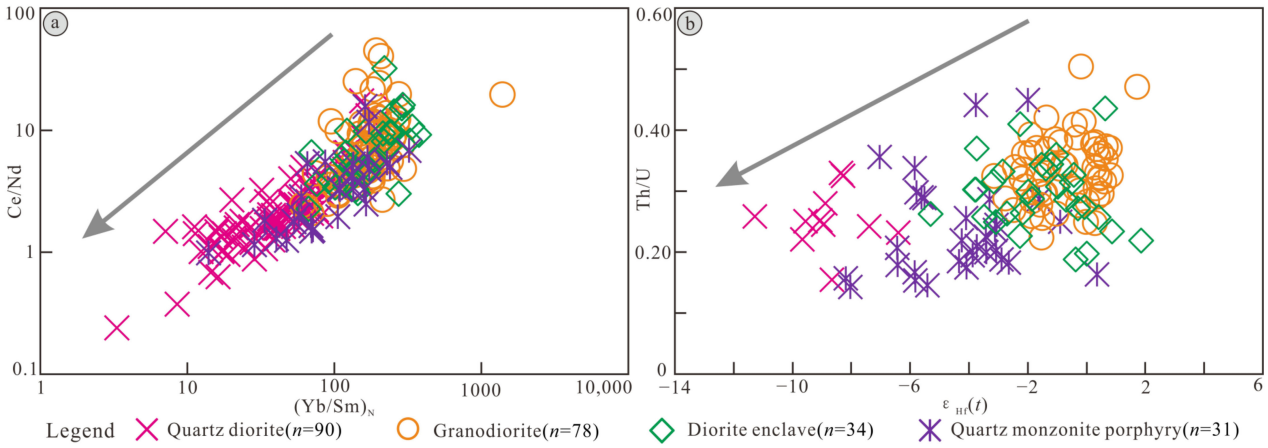

Figure 12. The (**a**) Ce/Nd vs. $(Yb/Sm)_N$ ratios and (**b**) Th/U vs. $\varepsilon_{Hf}(t)$ variation diagrams for studied zircons in the Yangla granitoid intrusions. The data of quartz monzonite porphyry, granodiorite, and dioritic enclaves referred the Meng et al. (2016) [3].

5. Discussion

Zircon ($ZrSiO_4$) is an important accessory mineral in granitoids, and absorbs various trace elements during its crystallization process (such as REE, U, Th, and Ti) [26,62,69]. Laser-ablation inductively-coupled-plasma-mass-spectrometry (LA-ICP-MS) has made it possible to analyze trace element concentrations in zircons, along with U–Pb dating [51]. Previously published research has suggested the geochemistry of trace elements

in zircons, in spite of the wide range of contents, can produce a very significant set of information useful for metallogenetic, petrogenetic, geochronological, and provenance studies [3,19–23,26,51,70,71]. Currently, the trace elements in zircons have been widely used to estimate the crystallization temperature and oxygen fugacity, determine magma source and crustal sediments assimilation, constrain the separation and crystallization of minerals and analyze the metallogenic potential of intrusions [62–69,71–73].

5.1. Magma Source

Zircons have good stability and are an important tool for exploring crustal evolution and tracing rock source areas. Moreover, zircons usually have higher Hf concentrations (0.5–2.0%) and lower Lu concentrations, resulting in low Lu/Hf ratios. Therefore, there is no obvious accumulation of radioactive Hf in zircon after its formation, and the Hf isotopic values of the initial system of zircon formation can be accurately obtained [15,46]. Furthermore, the Hf isotopic composition of the zircon parent melt is difficult to reset after the formation system is closed and is not affected by another geological process [74]; thus, the heterogeneity of zircon Hf isotopic values is related to the magma source and records useful origin information [2]. In particular, the t^{C}_{DM} values can better record and reflect source materials region information, such as the time of source materials being extracted from the depleted mantle or remaining in the crust, because of relatively lower zircon $f_{Lu/Hf}$ values of Yangla granitoids plutons [75].

The quartz diorite samples have $(^{176}Hf/^{177}Hf)_t$ values of 0.282332–0.282470 (avg. 0.282403), and the $\varepsilon_{Hf}(t)$ are −11.28 to −6.40 (avg. −8.77). The quartz diorite samples primarily plot near the evolution line of the lower crust in $(^{176}Hf/^{177}Hf)_t$ and diagenetic chronology diagrams (Figure 13a,b). The quartz diorite samples also primarily plot near the evolution line of the lower crust in diagrams of $\varepsilon_{Hf}(t)$ and diagenetic chronology (Figure 13c,d), indicating that the source region may be the negative $\varepsilon_{Hf}(t)$ values component of the lower crust. Therefore, Figure 13 indicates that the parent magma of the quartz diorite may have mainly derived from the melting of ancient lower crustal materials [15,75,76]. Furthermore, the corresponding T^{C}_{DM} of quartz diorite is 1.6–2.0 Ga, with an average of 1.8 Ga, which also suggests that the magma may originate from ancient Paleoproterozoic lower crustal material.

The quartz monzonite porphyry samples have $(^{176}Hf/^{177}Hf)_t$ values of 0.282396–0.282617 (avg. 0.282508), and the $\varepsilon_{Hf}(t)$ are −8.18 to 0.37, with only one sample being positive, and the others being negative, with an average of -4.29. The quartz monzonite porphyry samples primarily plot within the region between lower crustal materials and chondrite evolution lines in the $(^{176}Hf/^{177}Hf)_t$ and chronology diagrams (Figure 13a,b). These samples also primarily plot within the region between lower crustal materials and the chondrite evolution lines in the $\varepsilon_{Hf}(t)$ and chronology diagrams (Figure 13c,d), and the corresponding t^{C}_{DM} are concentrated between 1.2 and 1.8 Ga, with an average of 1.5 Ga, suggesting that the magma may originate from Paleo-Mesoproterozoic components of the lower crust. Granodiorite and dioritic enclaves have similar Lu-Hf isotopic composition values, including similar $\varepsilon_{Hf}(t)$ and t^{C}_{DM} values. The $\varepsilon_{Hf}(t)$ values are concentrated between −8.6 and +2.8, dominated by negative values (only a few are positive), and the t^{C}_{DM} values are concentrated between 1.1 and 1.8 Ga, indicating that they may have consistent magma source regions. Granodiorite and dioritic enclave samples primarily plot in the region between the lower crust and chondrite evolution lines, and a small number of samples plot in the upper regions of the chondrite evolution line in the $(^{176}Hf/^{177}Hf)_t$ and chronology diagrams (Figure 13a,b). The granodiorite and dioritic enclave samples also primarily plot in regions between the lower crust and the chondrite evolution lines, and a small number of samples ($\varepsilon_{Hf}(t) > 0$) plot in the upper regions of the chondrite evolution line in the $\varepsilon_{Hf}(t)$ and chronology diagrams (Figure 13c,d); this indicates a potentially heterogeneous magma source, where ancient Mesoproterozoic negative $\varepsilon_{Hf}(t)$ value components may have been mixed with newborn positive $\varepsilon_{Hf}(t)$ value components [3]. The negative and positive $\varepsilon_{Hf}(t)$ values usually show the characteristics of crustal melting and mantle-derived magma or

new crustal material components, respectively [2,77]. However, previous studies have pointed out that most of the negative $\varepsilon_{Hf}(t)$ values of the granodiorite in the Yangla mining district mainly originate from Paleo-Mesoproterozoic continental crustal materials and a small number of positive $\varepsilon_{Hf}(t)$ values represent a certain mixing proportion of mantle-derived materials, resulting in an inhomogeneous isotopic composition of the magma source region, which is a mixed magma formed by crust-mantle interaction [2,3,5]. Moreover, a large number of mafic microgranular enclaves (MME) and Sr-Nd-Pb-O isotopic features of the granodiorite plutons further confirm that mantle-derived components contribute to the magma system without contamination by new crustal materials at Yangla [2]. Therefore, the magma of the granodiorite and dioritic enclaves may have originated from lower crust Paleo-Mesoproterozoic material, combined with contaminations of mantle-derived material components in the deep lower crust, and crust-mantle interactions that occurred to form a mixed magma [2,33]. This has similar magma origin characteristics to the Yidun island arc belt granitoids in the southwest Sanjiang region to the east, which also originated from the remelting of Paleo-Mesoproterozoic material components in the lower crust, accompanied by mantle-derived components added to form a mixed magma [78–80].

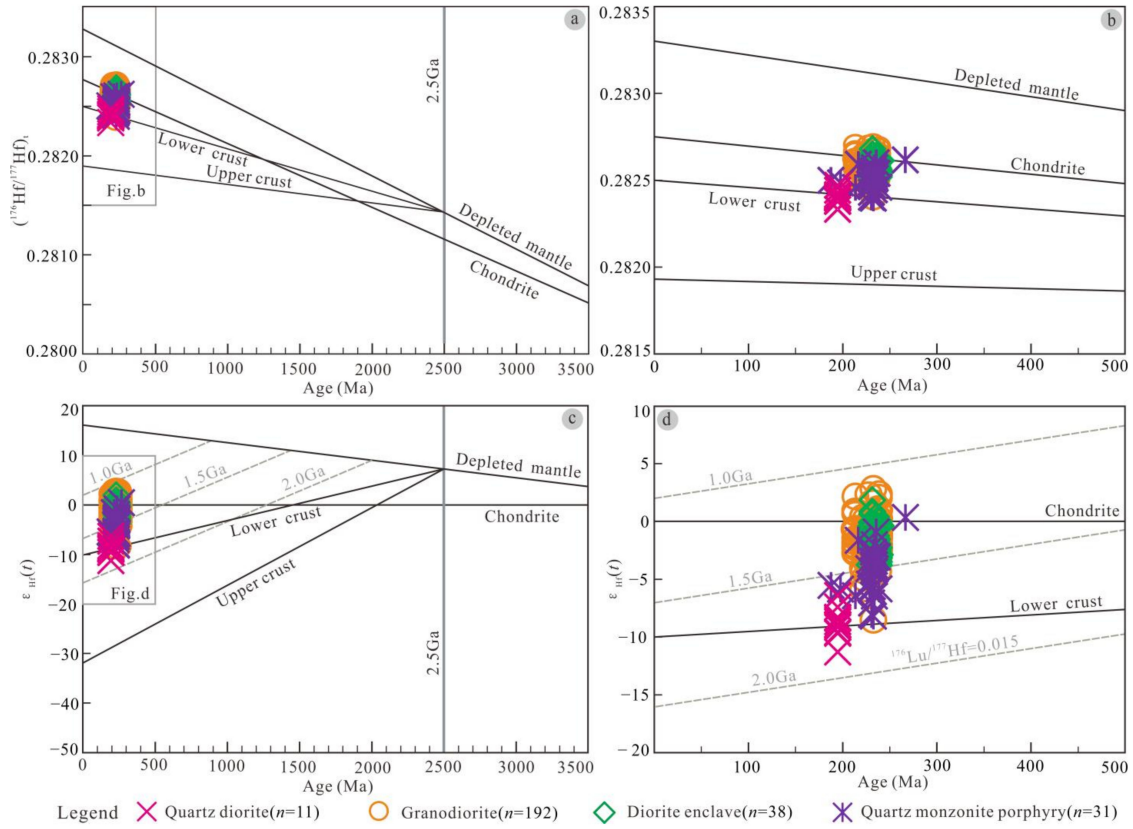

Figure 13. Hafnium isotopic compositions and zircon U-Pb ages plots from Yangla granitoid intrusions. (**a**,**b**) $^{176}Hf/^{177}Hf$ vs. zircon U-Pb age; (**c**,**d**) $\varepsilon_{Hf}(t)$ vs. zircon U-Pb age. The Yangla granitoid intrusions data after the references [2–5]. These original diagrams were obtained from Ref. [15].

Regionally, the JOB was formed by the separation of the Qamdo-Simao Block (QSB) from the Yangtze Block (YB), and the basement materials of the JSZ and QSB should be consistent with those of the YB [2,81]. Greentree et al. (2006) [82] and Zhao et al. (2012) [83] have confirmed that the western YB basement mainly underwent numerous tectono-magmatic and metamorphic events at 2700–2600, 2500–2400, 2000–1900, 1100–1000, and 910–720 Ma. However, the t^{C}_{DM} of the quartz diorite, quartz monzonite porphyry, and granodiorite—dioritic enclaves are 1500–2000, 1200–1800, and 1100–1800 Ma, respectively, and none of them correspond to obvious igneous and metamorphic events in the YB. In addition, Neoproterozoic basement mafic rocks at the western

margin of the YB usually have positive $\varepsilon_{Hf}(t)$ values (~12.0), suggesting that Neoproterozoic materials were added to the crust at that time [84]. The Lunong and Jiangbian granodiorite intrusions of Yangla and the Neoproterozoic mafic rocks at the western margin of the YB have a partially similar distribution range of Hf isotopic composition, indicating the existence of Neoproterozoic crustal materials that were added to the Triassic acidic magmatic system and participated in the diagenesis process of granitoids in Yangla [3]. Therefore, the magma may primarily originate from Paleo-Meso-Neoproterozoic materials in the lower crust, coupled with a small amount of mantle-derived components contamination in the YCWPD.

Studies have suggested that the Yangla granodiorite is an I-type granite [2], whereas the quartz diorite is an S-type granite [14]. I- and S-type granites primarily originated from the partial melting process of the pre-existing lower crustal igneous rocks and upper crustal sediments, respectively [77,85]. However, previous studies on zircon Hf-O isotopic values have suggested that I- and S-type granites can also be formed by the mixing of magma with different proportions of mantle-derived components and remelted crustal sedimentary material [77,86]. Given that the quartz diorite, quartz monzonite porphyry, granodiorite, and dioritic enclave were mainly derived from two source regions (mantle and lower crustal materials), the Hf-O-Pb isotopic compositions of GR further indicate that the evolution and diagenesis of the magmatic system involved mixing with upper crustal sediments; hence, these magmas may be involved three-component upper crust + lower crust + mantle mixing materials [2]. Moreover, studies have confirmed that the granitoids plutons (i.e., quartz diorite, quartz monzonite porphyry, granodiorite, and dioritic enclave) are the products of the same magmatic diagenesis system at Yangla region [2,3,5,13] and the differences in diagenetic chronology can be attributed to multiphase emplacement [3]. Therefore, the Yangla granitoids plutons should have the same magma source region, which is mainly derived from three-component mixing magmas, these components being upper crustal sediments + lower crustal Paleo-Meso-Neoproterozoic materials + mantle-derived components.

5.2. Assimilation and Fractional Crystallization

5.2.1. Assimilation

Many magmas assimilate wall rock during their residence in the crust, and crustal assimilation of magmas deriving from various degrees of crustal assimilation could lead to distinct zircon trace element trends with magma compositional evolution [87]. The chemical effects of crustal assimilation are most obvious in S-type granites, which assimilate large amounts of metasediment and consequently show higher aluminosity and more reduced chemistry [87]. The Yangla quartz diorite and granodiorite were mainly plotted within the slightly metaluminous to peraluminous and metaluminous to slightly peraluminous in the A/NK-A/CNK binary discrimination diagrams, respectively [2,14], which suggested the crustal assimilation may be responsible for the above-mentioned plutons geochemistry. Furthermore, if the magmatic system is contaminated by crustal sediments, which have distinctive high $\delta^{18}O$ values [88], reduced chemistry based on the Ce anomaly [89], and elevated concentrations of P [90] in zircon grains. Bell et al. (2019) [91] and Bell and Kirkpatrick (2021) [87] further confirmed that the sediment assimilation is supported by the higher $\delta^{18}O$, lower oxygen fugacity (fO_2), and higher P contents within zircons. The zircon oxygen $\delta^{18}O$ values of Yangla granodiorite mainly range from 7 to 9‰ (Avg. 8.0‰; Figure 14a) and are significantly higher than the transition-eastern and western zone plutons and relatively lower than high-Sr/Y plutons in Peninsular Ranges Batholith PRB of Baja California and Southern California, which indicated that there is obvious assimilation of crustal metasediments [87]. Zircon P concentrations of Yangla quartz diorite are significantly higher than that of plutons in PRB (Figure 14b), which suggests that the Yangla granitoids plutons probably contain a considerable assimilated metasedimentary component. The oxygen fugacity (fO_2) of Yangla granitoids plutons is roughly consistent with that of plutons in PRB (Figure 14c), which also indicates that Yangla granitoids plutons assimilate large amounts of metasediments. The above-mentioned variation pattern is also supported by the zircons (i.e., elevated LREE contents and increasing average Nd/Dy

ratios) and whole rock geochemistry (i.e., more radiogenic $^{87}Sr/^{86}Sr$, less radiogenic ε_{Nd}, and higher Pb isotope ratios) in PRB of southern California and Baja California [87,92]. The LREE concentrations and Nd/Dy ratios show slightly increase from dioritic enclave and granodiorite, through quartz monzonite porphyry, and to quartz diorite (Figure 15), which indicates that there are obvious sediments assimilation and the degree of sediments contamination gradually increased in the Yangla magmatic system. Zhu et al. (2011) [2] have revealed whole rock Sr, Nd, and Pb isotopic compositions of Beiwu, Linong, and Lunong granodiorite and $(^{87}Sr/^{86}Sr)_i$, $\varepsilon_{Nd}(t)$, $^{206}Pb/^{204}Pb$, and $^{208}Pb/^{204}Pb$ mainly range from 0.7078 to 0.7148 (avg. 0.7095), and −6.70 to –5.10 (avg. −6.0), 18.213 to 18.598 (avg. 18.407), and 38.323 to 38.791 (avg. 38.601), respectively. These whole rock Sr, Nd, and Pb isotopic compositions of Yangla granodiorite are roughly consistent with the PRB plutons (i.e., avg. $^{87}Sr/^{86}Sr$ = 0.704, ε_{Nd}=-5.0, $^{206}Pb/^{204}Pb$ =18.787, and$^{208}Pb/^{204}Pb$ = 38.445; [93]), suggesting that Yangla plutons have assimilated continental materials (i.e., sediments and/or metasediments). Moreover, we also referred to whole rock chemistry of the "hybridization index" (FeO^T + MgO + TiO_2 + MnO) for comparison with K_2O, Na_2O, U, Th, Ba, Rb, Nb, and Ta contents of Yangla quartz diorite and granodiorite [2,14]. There are identifiable correlations between the hybridization index and K_2O, Na_2O, U, Th, Ba, Rb, Nb, and Ta [2,14], and indicate contamination of granitic magma by metasedimentary rock caused by chemical interaction with the granitoids [24].

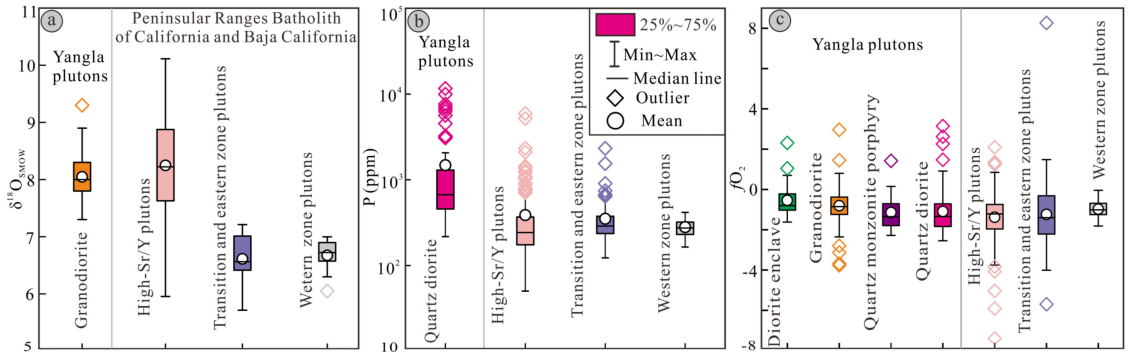

Figure 14. The zircons (**a**) oxygen isotopic composition, (**b**) P concentrations, and (**c**) oxygen fugacity diagram of Yangla granitoids plutons and Peninsular Ranges Batholith. The zircon $\delta^{18}O$ values of granodiorite sourced by Zhu et al. (2011) [2]; The $\delta^{18}O$ values, P concentrations, and oxygen fugacity (fO_2) of the high-Sr/Y, transition and eastern zone, and western zone plutons were referred from the Bell et al. (2019) [91] and Bell and Kirkpatrick (2021) [87].

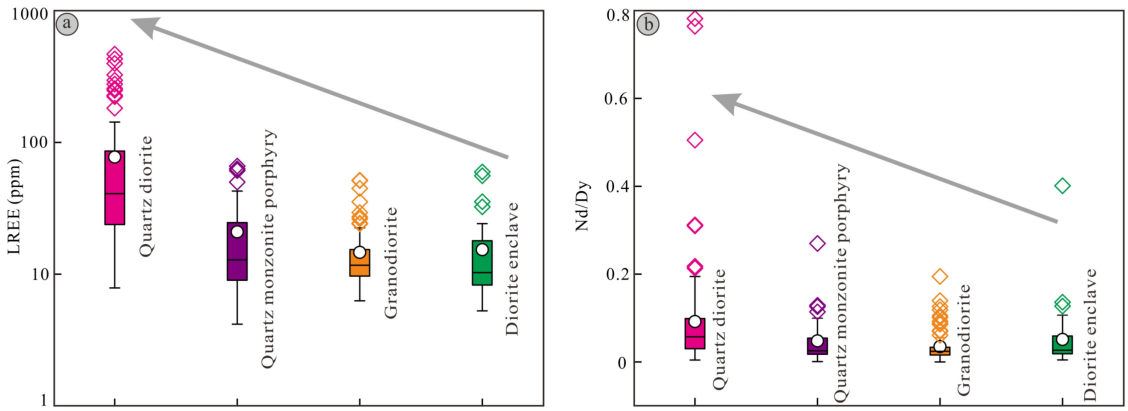

Figure 15. The zircons (**a**) light rare earth element and (**b**) Nd/Dy ratios variation diagram of Yangla granitoids plutons. The data on quartz monzonite porphyry, granodiorite, and diorite enclave was sourced from Meng et al. (2016) [3].

Consequently, we preliminary believe that Yangla granitoid plutons have assimilated crustal metasediments, and the degree of sediment assimilation shows a gradual increase from dioritic enclave and granodiorite through quartz monzonite porphyry and to quartz diorite.

5.2.2. Fractional Crystallization

The variations of zircons trace element compositions can well reflect the degree of magma differentiation and the crystallization of accessory minerals during the crystallization and differentiation process [24,69,94]. Studies suggest the contents of incompatible elements (i.e., Th, U, Y, and REE) in residual magma will gradually increase, coupled with the increased degree of magmatic crystallization fractionation, and these characteristics will be recorded by the zircons from the magmatic system [69,73,95]. The contents of ΣREE, Th, U, and Y in the four stages of magmatic zircons gradually increased in the Yangla deposit (Figure 16a–c), showing that the fractionation of the Yangla granitoids plutons gradually increased from the early to late stage. Furthermore, if there were separated and crystallized MREE-rich minerals (i.e., apatite, titanite, and hornblende) in the early stage of magmatic evolution, the residual melt would relatively lose REE (i.e., Sm and Gd) and then the Ce/Sm and Yb/Gd ratios will simultaneous increased [96]. Figure 16d shows that the four stages of magmatic rocks in the Yangla deposit have undergone significant crystallization differentiation of apatite, titanite, and hornblende during the diagenesis process. In particular, the positive correlation between P and Y in quartz diorite zircons further confirms the existence of apatite separation and crystallization in Figure 16e [69]. Moreover, the Ta and Nb of dioritic enclaves, quartz diorite, and quartz monzonite porphyry zircons show a significant positive correlation in Figure 16 f, indicating that the source region may undergo obvious rutile crystallization and differentiation process [69]. There is no clear correlation between Ta and Nb in granodiorite zircons, indicating that there may be no separation and crystallization of rutile that formed the granodiorite magma.

In summary, the trace elements variations of zircons indicated that the Yangla granitoids plutons (dioritic enclaves, quartz monzonite porphyry, and quartz diorite) mainly experienced the separation and crystallization of apatite, titanite, hornblende, and rutile. The Yangla granodiorite plutons mainly experienced the separation and crystallization of apatite, titanite, and hornblende. These results are consistent with the mineralogical characteristics of apatite, titanite, and rutile as the accessory minerals and hornblende as the main minerals of the Yangla granitoid plutons [2–5,14]. The degree of magma differentiation gradually increased from dioritic enclaves and granodiorite through quartz monzonite porphyry and to quartz diorite, corresponding to the early to late stages of magmatic evolution in the Yangla mining district.

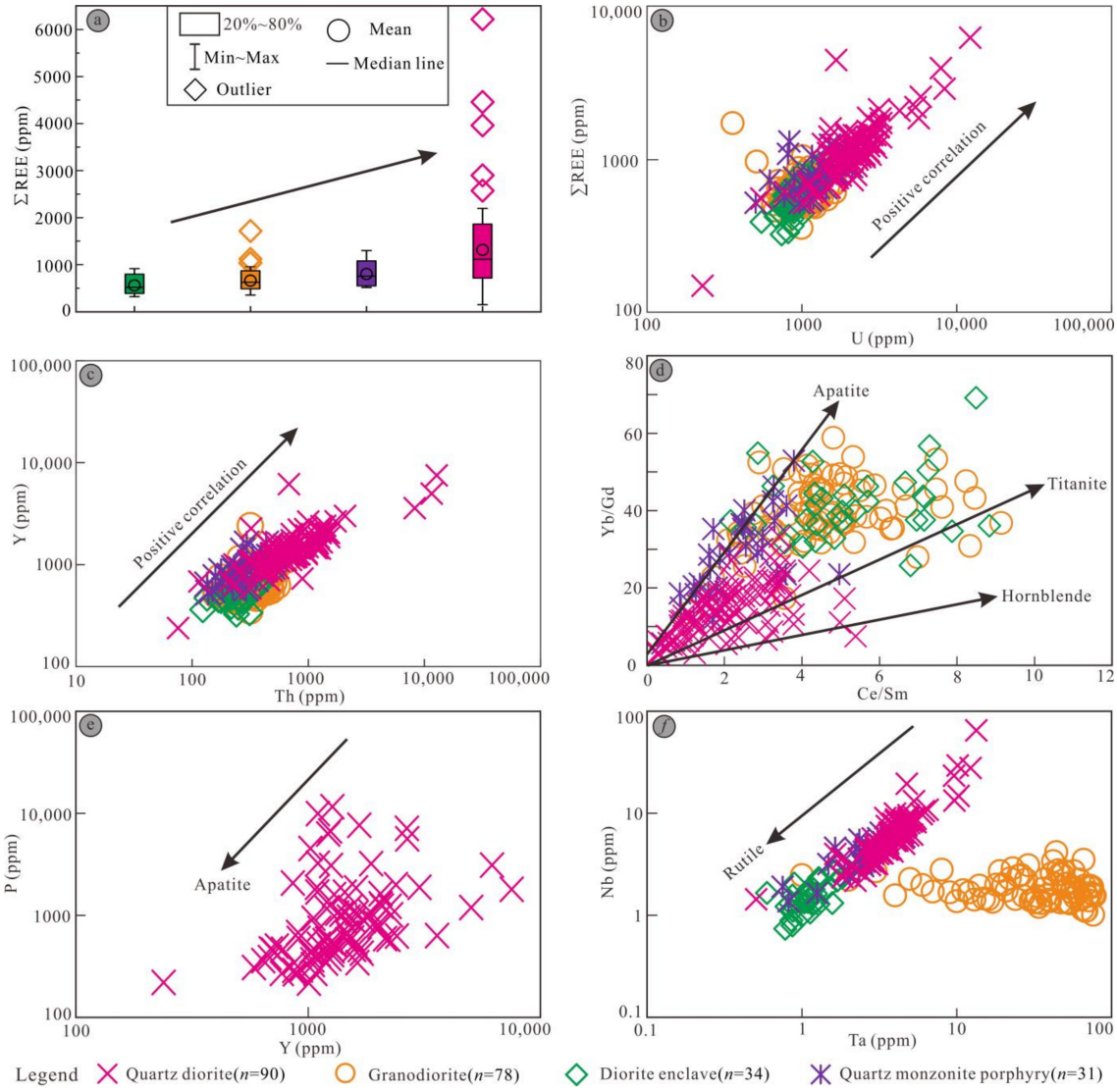

Figure 16. The indication diagram of magmatic zircons trace elements on magmatic mineral fractional crystallization of Yangla granitoid plutons. The dioritic enclaves, granodiorite, and quartz monzonite porphyry zircons data from Ref. [3]. (**a**) the comparative box plots for the zircons ∑REE; (**b**) the binary diagram of zircons ∑REE vs. U; (**c**) the binary diagram of zircons Y vs. U; (**d**) the binary diagram of zircons Yb/Gd vs. Ce/Sm; (**e**) the binary diagram of zircons P vs. Y; (**f**) the binary diagram of zircons Nb vs. Ta.

5.3. Magmatic Evolutionary Sequence

The geochronology of the Yangla granitoids shows an obvious decrease from dioritic enclave (~232 Ma) through granodiorite (~208 Ma) and quartz monzonite porphyry (~202 Ma) and to quartz diorite (~195 Ma). Combined with the diachronous collision-closure process and tectonic setting of the JOB, indicating that the corresponding magmatic activity in the YCWPD may have lasted up to 33 Ma [35], and various granitoids formed via "multiphase emplacement" of the same magmatic system [3]. Furthermore, Yangla granitoids are the products of different evolution stages of the same magmatic system formed by the partial melting and (or) fractional crystallization action [2,14]. Studies have verified that the $^{176}Hf/^{177}Hf$ ratios gradually decrease owing to the continuous addition of continental crustal materials during the evolution of the magmatic system [77], which usually corresponds to the evolution of the magmatic system from an early to late stage. Given that the $^{176}Hf/^{177}Hf$ ratios of the Yangla granitoids show the various features of quartz diorite

< quartz monzonite porphyry < granodiorite and dioritic enclaves, this further clarifies the notion that the granitoids are the products of different evolutionary stages in the Yangla mining district (Table 2; Figure 9c), which also supported by the evidence of petrography about the above-mentioned intrusions. The variation in $^{176}Hf/^{177}Hf$ ratios indicates that the mid-to-late Triassic granodiorite and dioritic enclaves were followed by the quartz monzonite porphyry, which was in turn followed by the Late Triassic to Early Jurassic quartz diorite, and the crustal materials mixed into the magmatic system gradually increased. This is also consistent with the $\varepsilon_{Hf}(t)$ values of the quartz diorite are all negative; the quartz monzonite porphyry has only one positive value, and the granodiorite and dioritic enclaves are primarily negative, with a few positive values. Moreover, Meng et al. (2016) [3] have proposed the magma which resulted in the formation of quartz monzonite porphyry is a later and more evolved melt stage compared to the granodiorite, which, based on a good correlation (i.e., both ratios decline with progressive magmatic evolution) between Th/U and Zr/Hf ratios in zircons. This evolving pattern can be further supported by the elevated LREE and HREE contents of the studied zircons from quartz diorite, quartz monzonite porphyry, granodiorite, and dioritic enclaves in the Yangla deposit. As seen in the binary diagrams for Ce/Nd vs. $(Yb/Sm)_N$ (Figure 12a), the HREE relative to LREE enrichment decreases systematically from granodiorite and dioritic enclaves through quartz monzonite porphyry and to quartz diorite (although overlaps in Figure 15a), showing an evolutionary process from early to later magmatic stage. Furthermore, the $\varepsilon_{Hf}(t)$ values of the zircons Yangla granitoids have a positive correlation with Th/U ratios (although they overlap in Figure 12b), with the Th/U ratios being proxies for the degree of differentiation [77]. This positive correlation between $\varepsilon_{Hf}(t)$ and Th/U ratios revealed the progressive evolution from dioritic enclaves and granodiorite through quartz monzonite porphyry and to quartz diorite, which indicated the magmatic system increasingly assimilated crustal components throughout its evolution [3]. In addition, Meng et al. (2016) [3] have confirmed the rare xenocrystic zircons observed in the quartz monzonite porphyry, which further supported the assimilated crust materials within the magmatic system. Therefore, our preliminary interpretation is that during the the evolution of magma with a continuation of assimilation and fractional crystallization, the contamination amount of upper crustal metasediments gradually increased, and dioritic enclaves, granodiorite, quartz monzonite porphyry, and quartz diorite were formed in sequence, corresponding to the early to late stages of Yangla magmatic system evolution.

5.4. Metallogenic Potential

Currently, zircon has become an effective indicator mineral to judge the mineralization potential of granitoids intrusions, which is based on the continuous improvement of trace element analytic technology (i.e., LA-ICP-MS) [66,73,97,98]. Ballard et al. (2002) [19] suggested that Cu mineralization is directly associated only with intrusions with zircon δ Eu > 0.40 (Figure 17), which is based on the barren and fertile calc-alkaline intrusions from Chuquicamata El Abra porphyry copper belt of northern Chile. The zircon δ Eu values of Yangla quartz diorite are mainly concentrated between 0.5 and 1.2, with an average of 0.90, and significantly higher than 0.4 and indicates the quartz diorite has good Cu metallogenic potential. The zircon δ Eu values of quartz monzonite porphyry, granodiorite, and dioritic enclaves mainly range from 0.2 to 0.50 (avg. 0.4), 0.2 to 0.4 (avg. 04), and 0.2 to 0.40 (avg. 0.50) (Figure 17), respectively. These zircons δ Eu values of Yangla granitoids roughly similar to the intrusions in the Zhongdian ore concentrated area of SW China (i.e., Relin, Tongchanggou, Disuga, and Pulang; [67]), Jiangnan orogen belt of China (Dexing; [66]), Hualgayoc mining district of northern Peru [49], and Chuquicamata El Abra porphyry copper belt of northern Chile [19] (Figure 17), suggesting that Yangla granitoids have a good potential for Cu mineralization. In particular, the Xiuwacu deposit was dominated by the tungsten and shows slightly lower δ Eu values in the Zhongdian ore concentrated area of SW China [67], and generally similar to the Yangla granitoids (i.e., quartz monzonite

porphyry, granodiorite, and dioritic enclaves) [3]. It further indicates that Yangla granitoids also have tungsten metallogenic potential.

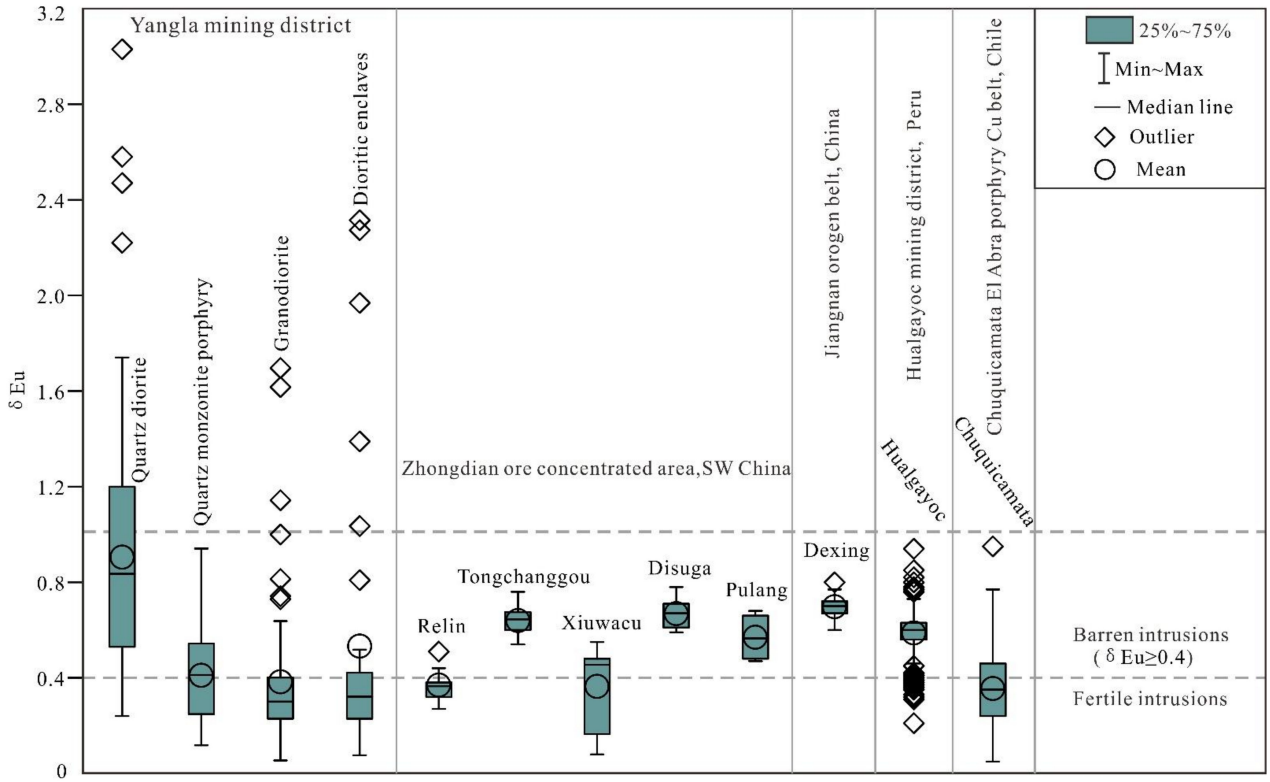

Figure 17. The zircon δEu values for Yangla granitoid plutons and other ore-related intrusions. Data for Yangla quartz monzonite porphyry, granodiorite, and dioritic enclaves from Meng et al. (2016) [3]; Data for Zhongdian ore concentrated area intrusions, SW China from Li et al. (2022) [67]; Data for Dexing porphyry Cu deposit intrusions from Zhang et al. (2017) [66]; Data for Hualgayoc mining district intrusions (Peru) from Viala and Hattori (2021) [49]; Data for Chuquicamata El Abra porphyry copper belt intrusions (Chile) from Ballard et al. (2002) [19].

Lu et al. (2016) [22] further research suggested that the fertile magmatic suites have collectively higher δEu > 0.30, 10,000*(Eu/Eu*)/Y (>1.0), (Ce/Nd)/Y (>0.01), and lower Dy/Yb (<0.3) ratios than infertile suites which based on the zircon compositions as a pathfinder for porphyry Cu ± Mo ± Au deposits. In particular, zircon (Eu/Eu*)/Y ratios are positively correlated with (Ce/Nd)/Y ratios in the fertile suites, but this correlation is lacking in the infertile suites. The zircon δEu values of most Yangla quartz diorites are greater than 0.30. Only one sample spot of Yanla quartz diorite has a 10,000*(Eu/Eu*)/Y ratio lower than 1.0, and the others have greater than 1.0. Most quartz diorite zircons also show (Ce/Nd)/Y and Dy/Yb ratios greater and lower than 0.01 and 0.30, respectively. Furthermore, there is a slightly positive correlation between (Eu/Eu*)/Y and (Ce/Nd)/Y ratios in quartz diorite. Therefore, we preliminarily believe that Yangla quartz diorite has Cu mineralization potential. Moreover, the other Yangla granitoids (i.e., quartz monzonite porphyry, granodiorite, and dioritic enclaves) have similar features with the quartz diorites in zircon δ Eu, 10,000*(Eu/Eu*)/Y, (Ce/Nd)/Y, and Dy/Yb values [3], which also indicate these granitoids have a good Cu metallogenic potential in the Yangla mining district.

Geng et al. (2019) [98] have proposed the discriminant diagram between ore-forming and barren granitoids intrusions based on zircons REE compositions of big data mining, such as the binary Eu/Dy × 100 vs. Ce/Nd × 0.1 (Figure 18a), Er/Lu vs. Ce/Sm (Figure 18b), Er/Lu vs. Dy/Yb × 10 (Figure 18c), Er/Lu vs. Dy/Lu (Figure 18d), Er/Yb × 10 vs. Gd/Dy × 10 (Figure 18e), Er/Lu vs. Tb/Tm × 10 (Figure 18f), and the triangular Eu/Gd × 100-Eu/Dy × 100-Gd/Yb × 100 (Figure 18g) and Eu/Gd × 100-Dy/Yb × 10-Er/Yb × 10 (Figure 18h). These binary and ternary

discriminant diagrams can effectively distinguish the mineralization types of granitoids, such as Cu and W. Most Yangla granitoids (i.e., granodiorite, dioritic enclaves, quartz monzonite porphyry, and quartz diorite) mainly plotted within the Cu-related intrusions in Figure 18, suggesting that these granitoids have great potential for Cu mineralization, which is consistent with the geological fact that the Yangla deposit is dominated by Cu [1]. Moreover, a few Yangla granitoids samples are plotted within the W-related intrusions regions, indicating that these granitoids also have a certain W metallogenic potential, which is consistent with the geological facts of the newly discovered tungsten orebodies in the depth of the Yangla deposit (Figure 19) [99]. Furthermore, the Cu and W contents of the quartz diorite mainly range from 2019 to 12,170 ppm (avg. 6466 pm) and 79 to 1103 ppm (avg. 492 ppm) (Table 4; [32]), respectively, which also indicated that the quartz diorite has a certain Cu-W metallogenic potential.

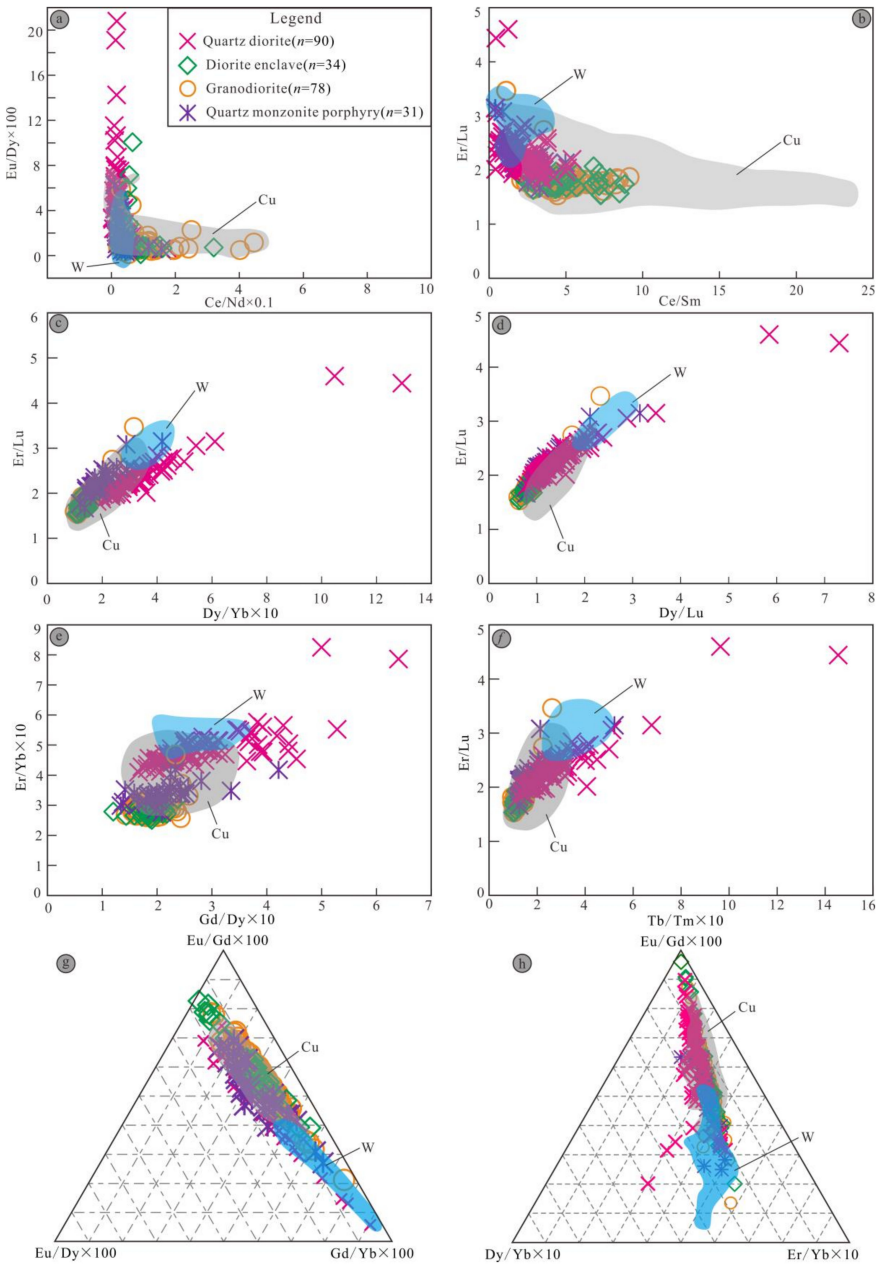

Figure 18. The binary (**a**–**f**) and triangular (**g**,**h**) metallogenic potential discriminant diagrams of zircon trace elements from Yangla granitoid plutons. The dioritic enclaves, granodiorite, and quartz monzonite porphyry zircons data from Ref. [3]. The region data of Cu and W referenced the [98].

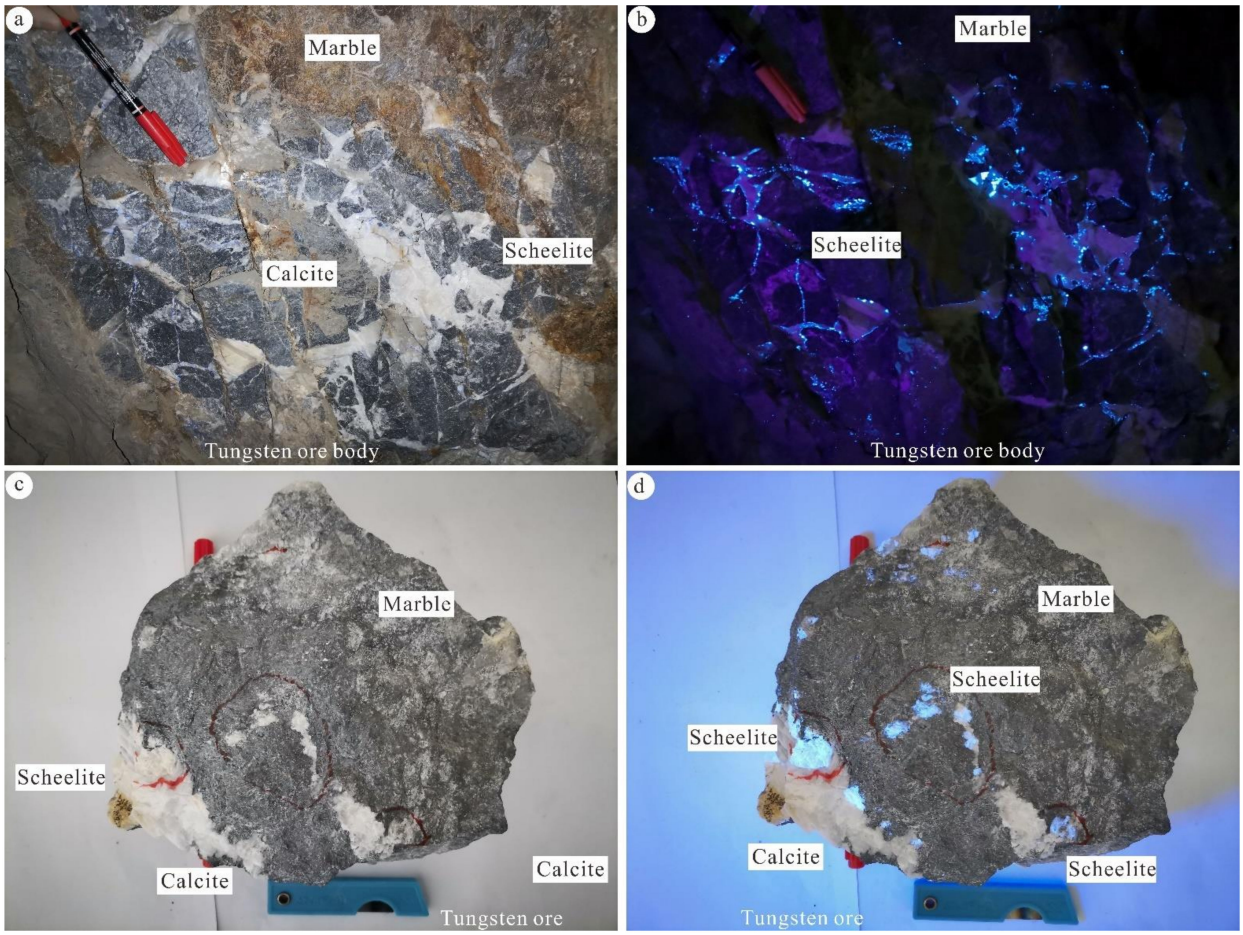

Figure 19. The photos of tungsten mineralization in the Yangla Cu-W polymetallic deposit. (**a**) and (**b**) the photographs of tungsten ore body with the host second sequence of Linong Formation; (**c**) and (**d**) the photographs of hand specimen of scheelite with the host marble.

Table 4. The metallogenic elements (Cu and W) concentrations of quartz diorite in the Yangla Cu-W polymetallic deposit.

Sample No.	Cu/ppm	W/ppm	Reference
3250-41-3	5209	1103	
3250-41-4	12,170	295	[32]
3250-41-5	2019	79	

Previous studies have shown that the lower Dy/Yb ratios (<1) of zircons in the ore-forming plutons usually show the H_2O-rich features of the magma system, and the Dy/Yb ratios of zircons in the W ore-forming pluton are less than 0.4, which are lower than Cu ore-forming plutons [73]. Experimental petrology shows that the Y/Ho ratios in crystallized zircons from granitic magma are positively correlated with the F concentration in the magma [100]. Tungsten (W) is often enriched in F-rich and highly fractionated magma as a typical high-field strength element [101]. Ye et al. (2022) [73] further proposed two binary discrimination diagrams for ore-bearing intrusion based on zircon variations of Dy/Yb and Y/Ho ratios, such as Dy/Yb vs. Y (Figure 20a) and Y vs. Y/Ho (Figure 20b). The Dy/Yb ratios of all granodiorite, dioritic enclaves, and most quartz monzonite porphyry and quartz diorite samples from the Yangla deposit are less than 0.4 in Figure 20a, indicating that these granitoids have the potential to form tungsten deposit. The Y/Ho ratios of all dioritic enclaves and most granodiorite, quartz monzonite porphyry, and a small number of quartz diorite samples are mainly plotted within the region of Y/Ho ratios greater than

28 (enriched F system) in the Figure 20b. Most quartz diorite samples are mainly plotted within the region of the Y/Ho ratios are less than 28 (enriched Cl system) in Figure 20b. Therefore, zircons Dy/Yb and Y/Ho ratios features further confirm that Yangla granitoids have the potential to form not only Cu but also W deposit.

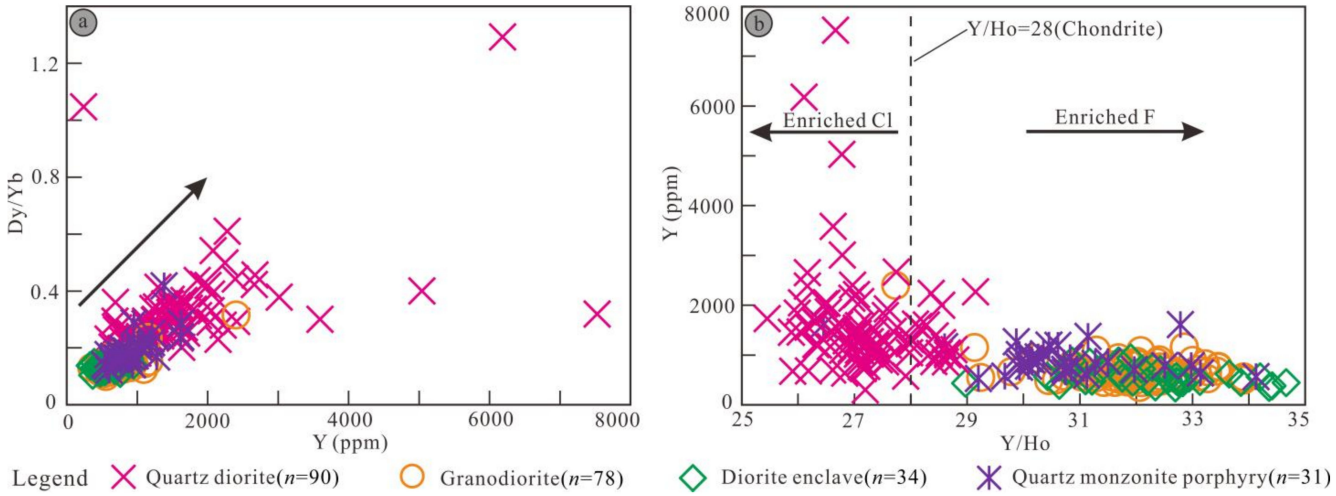

Figure 20. The metallogenic potential discrimination diagrams of zircon trace elements from Yangla granitoid plutons. The dioritic enclaves, granodiorite, and quartz monzonite porphyry zircons data from Ref. [3]. (**a**) the binary diagram of Dy/Ce vs. Y and (**b**) the binary diagram of Y vs Y/Ho.

Mao et al. (2020) [102] suggested the tungsten deposits mainly related to highly differentiated reductive S-type granite, followed by oxidized I-type granodiorite in the Jiangnan tungsten belt, south China. The Yangla granodiorite and quartz diorite pluton belong to the I- and S-type granite, respectively [2,14], and dioritic enclaves, granodiorite, quartz monzonite porphyry, and quartz diorite experienced strong mineral crystallization differentiation and the corresponding oxygen fugacity values gradually decreased, which were highly similar to the W-related granites in the Jiangnan tungsten belt. Therefore, we preliminary believe that Yangla granitoids have certain W metallogenic potential. Li et al. (2022) [67] suggested that the oxygen fugacity of the magma forming the Cu deposit was greater than that of the W deposit; Cu and W are mainly related to mantle-derived components and ancient crustal materials, respectively. Oxygen fugacity is a key factor in Cu mineralization because magma with high oxygen fugacity is more conducive to the transport of metal elements and sulfur from the mantle to the epithermal setting of the crust [103]. However, tungsten mainly tends to be enriched in the crust, and the various states of oxygen fugacity cannot change the valence of tungsten (W^{6+}), but the feldspar-sericitization in the magmatic-hydrothermal period and the release of Ca^{2+} from calcium-bearing wall rocks are conducive to W enrichment and formation W deposit [67]. The oxygen fugacity of the Yangla granitoids gradually decreased (Figure 11b), and the upper crustal components gradually increased from early to late stages (Figure 10b), corresponding to the dioritic enclaves → granodiorite → quartz monzonite porphyry → quartz diorite. Moreover, combined with the Yangla deposit, geological facts of the intrusions usually coupled with sericitization, and the marble in Devonian Linong Formation were the main host rocks. This further shows that the Yangla granitoids plutons have W metallogenic potential. To sum up, Yangla granitoids plutons have a good potential for Cu-W polymetallic mineralization.

6. Conclusions

- The crystallization temperature and oxygen fugacity of the magma show a gradually increased and decreased from dioritic enclaves and granodiorite through quartz monzonite porphyry and to quartz diorite in the Yangla mining district, respectively.
- Yangla granodiorite, dioritic enclaves, quartz monzonite porphyry, and quartz diorite have consistent magma sources, all of which originate from three-component upper crust + lower crust + mantle mixed magmas; the provenance is primarily Proterozoic basement components and a small quantity of mantle-derived materials.
- The degree of crustal metasediments assimilation and differentiation have gradually increased from dioritic enclaves and granodiorite through quartz monzonite porphyry and to quartz diorite. These granitoids plutons mainly experienced the separation and crystallization of apatite, titanite, and hornblende.
- Yangla granodiorite and dioritic enclaves, quartz monzonite porphyry, and quartz diorite were formed in the early, mid, and late stages of magmatic evolution, respectively.
- Yangla granitoids plutons have a better potential for Cu-W polymetallic deposits.

Supplementary Materials: The following supporting information can be downloaded at: https://www.mdpi.com/article/10.3390/min12111427/s1, Supplementary Table S1: LA-ICP-MS analytical results of zircon trace elements (ppm), Ti-in-zircon temperatures (T_{Ti}/°C), and oxygen fugacity parameters (ΔFMQ) in the Yangla quartz diorite.

Author Contributions: Conceptualization, X.W. and B.L.; methodology, G.T.; formal analysis, G.T.; investigation, G.T., Z.L. and H.C.; data curation, Z.L.; writing—original draft preparation, X.W.; writing—review and editing, X.W. and B.L. All authors have read and agreed to the published version of the manuscript.

Funding: This study is supported financially by the National Natural Science Foundation of China (No. 41862007), the Key Disciplines Construction of Kunming University of Science and Technology (No. 14078384), and the Yunnan Ten Thousand Talents Plan Young & Elite Talents Project (YNWR-QNBJ-2018-093).

Data Availability Statement: The data used to support this study are included within the article.

Acknowledgments: We sincerely thank the Editorial Board members and anonymous reviewers for their constructive comments.

Conflicts of Interest: The authors declare that they have no known competing financial interest or personal relationships that could have appeared to influence the work reported in this paper.

References

1. Li, B.; Wang, X.F.; Tang, G.; Liu, Y.D.; Zou, G.F. S-Pb isotopes and tectono-geochemistry of the Lunong ore block, Yangla large Cu deposit, SW China: Implications for mineral exploration. *Ore Geol. Rev.* **2021**, *136*, 104249. [CrossRef]
2. Zhu, J.J.; Hu, R.Z.; Bi, X.W.; Zhong, H.; Chen, H. Zircon U-Pb ages, Hf-O isotopes and whole-rock Sr-Nd-Pb isotopic geochemistry of granitoids in the Jinshajiang suture zone, SW China: Constraints on petrogenesis and tectonic evolution of the Paleo-Tethys Ocean. *Lithos* **2011**, *126*, 248–264. [CrossRef]
3. Meng, X.Y.; Mao, J.W.; Zhang, C.Q.; Zhang, D.Y.; Kong, Z.G.; Jia, F.D. The timing, origin and T-fO_2 crystallization conditions of long-lived magmatism at the Yangla copper deposit, Sanjiang Tethyan orogenic belt: Implications for post-collisional magmatic-hydrothermal ore formation. *Gondwana Res.* **2016**, *40*, 211–229. [CrossRef]
4. Wang, Y.B.; Han, J.; Zeng, P.S.; Wang, D.H.; Hou, K.J.; Yin, G.H.; Li, W.C. U-Pb dating and Hf isotopic characteristics of zircons from granodiorite in Yangla copper deposit, Deqin County, Yunnan, Southwest China. *Acta Petrol. Sin.* **2010**, *26*, 1833–1844, (In Chinese with English abstract).
5. Zhang, H.R.; Yang, L.Q.; He, W.Y.; Gao, X.; Wang, H.Q.; Zhang, S.Y. Geochronology and geochemistry of the Tongjige granodiorites in the Jinshajiang suture zone, SW China: Constraints on petrogenesis and tectonic evolution of the Palaeo-Tethys Ocean. *Geol. J.* **2021**, *56*, 1445–1463. [CrossRef]
6. Yang, F.; Yu, C.; Jian, R.T.; Yao, Z.H. Characteristics of Petrology, Geochemistry and U-Pb Dating of Zircon from the Jiangbian Pluton in the Yangla Copper Deposit, Western Yunnan. *Geoscience* **2020**, *34*, 215–232, (In Chinese with English abstract).
7. Chen, S.Y.; Gu, X.X.; Cheng, W.B.; Zhang, Y.M.; Zheng, L.; Peng, Y.W.; Liu, R.P. Characteristics of stable isotopic compositions and its geological significances of the Yangla copper deposit, northwestern Yunnan Province. *Acta Petrol. Sin.* **2013**, *29*, 1290–1300, (In Chinese with English abstract).

8. Zhu, J.J.; Hu, R.Z.; Richards, J.P.; Bi, X.W.; Zhong, H. Genesis and Magmatic-Hydrothermal Evolution of the Yangla Skarn Cu Deposit, Southwest China. *Econ. Geol.* **2015**, *110*, 631–652. [CrossRef]
9. Du, L.J.; Li, B.; Huang, Z.L.; Zhou, J.X.; Zou, G.F.; Yan, Z.F. Carbon-oxygen isotopic geochemistry of the Yangla Cu skarn deposit, SW China: Implications for the source and evolution of hydrothermal fluids. *Ore Geol. Rev.* **2017**, *88*, 809–821. [CrossRef]
10. Yang, X.A.; Liu, J.J.; Han, S.Y.; Zhang, H.Y.; Luo, C.; Wang, H.; Chen, S.Y. U-Pb dating of zircon from the Linong granodiorite, Re-Os dating of molybdenite from the ore body and their geological significances in Yangla copper deposit, Yunnan. *Acta Petrol. Sin.* **2011**, *27*, 2567–2576, (In Chinese with English abstract).
11. Xie, S.X.; Yang, L.Q.; He, W.Y.; Gao, X. Garnet trace element geochemistry of Yangla Cu deposit in NW Yunnan, China: Implications for multistage ore-fluid activities in skarn system. *Ore Geol. Rev.* **2022**, *141*, 104662. [CrossRef]
12. Wang, X.F.; Li, B.; Xiang, Z.P.; Yue, Y.; Tang, G. Chemical compositions of sulfides in the porphyry Cu ores, Yangla Cu deposit, Yunnan, China: Implication for ore genesis. *Acta Geochim.* **2020**, *39*, 947–972. [CrossRef]
13. Wang, X.F.; Li, B.; Guan, S.J.; Nadeau, O.; Tang, G. Mineralized Granitic Porphyry of the Yangla Copper Deposit, Western Yunnan, China: Geochemistry of Fluid Inclusions and H-O, S, and Pb isotopes. *Geofluids* **2020**, *2020*, 4391703. [CrossRef]
14. Li, B.; Wang, X.F.; Du, L.J.; Xiang, Z.P.; Tang, G.; Huang, Z.L. Zircon U-Pb ages and geochemistry of granite porphyries in the Yangla Cu deposit, SW China: Constraints on petrogenesis and tectonic evolution of the Jinshajiang suture belt. *Geofluids* **2020**, *2020*, 8852277. [CrossRef]
15. Wu, F.Y.; Li, X.H.; Zheng, Y.F.; Gao, S. 2007 Lu-Hf isotopic systematics and their applications in petrology. *Acta Petrol. Sin.* **2007**, *23*, 185–220, (In Chinese with English abstract).
16. Li, H.; Danišík, M.; Zhou, Z.K.; Jiang, W.C.; Wu, J.H. Integrated U–Pb, Lu–Hf and (U–Th)/He analysis of zircon from the Banxi Sb deposit and its implications for the low-temperature mineralization in South China. *Geosci. Front.* **2020**, *11*, 1323–1335. [CrossRef]
17. Hoskin, P.W.O.; Ireland, T.R. Rare earth element chemistry of zircon and its use as a provenance indicator. *Geology* **2000**, *28*, 627–630. [CrossRef]
18. Hanchar, J.M.; Westrenen, W.V. Rare Earth Element Behavior in Zircon-Melt Systems. *Elements* **2007**, *3*, 37–42. [CrossRef]
19. Ballard, J.R.; Palin, M.J.; Campbell, I.H. Relative oxidation states of magmas inferred from Ce(IV)/Ce(III) in Zircon: Application to porphyry copper deposits of Northern Chile. *Contrib. Mineral. Petrol.* **2002**, *144*, 347–364. [CrossRef]
20. Nardi, L.; Formoso, M.; Jarvis, K.; Oliveira, L.; Neto, A.; Fontana, E. REE, Y, Nb, U, and Th contents and tetrad effect in zircon from a magmatic-hydrothermal F-rich system of Sn-rare metal–cryolite mineralized granites from the Pitinga Mine, Amazonia, Brazil. *J. S. Am. Earth Sci.* **2012**, *3*, 34–42. [CrossRef]
21. Dilles, J.H.; Kent, A.J.R.; Wooden, J.L.; Tosdal, R.M.; Koleszar, A.K.; Lee, R.G.; Farmer, L.P. Zircon compositional evidence for sulfur-degassing from ore-forming arc magmas. *Econ. Geol.* **2015**, *110*, 241–251. [CrossRef]
22. Lu, Y.J.; Loucks, R.T.; Fiorentini, M.; Mccuaig, T.C.; Evans, N.J.; Yang, Z.M.; Hou, Z.Q.; Kirkland, C.L.; Parra-Avila, L.A.; Kobussen, A. Zircon compositions as a pathfinder for porphyry Cu ± Mo ± Au deposits. *Soc. Econ. Geol. Spec. Publ.* **2016**, *19*, 329–347.
23. Loader, M.A.; Wilkinson, J.J.; Armstrong, R.N. The effect of titanite crystallisation on Eu and Ce anomalies in zircon and its implications for the assessment of porphyry Cu deposit fertility. *Earth Planet. Sci. Lett.* **2017**, *472*, 107–119. [CrossRef]
24. Yuan, F.; Liu, J.J.; Carranza, E.J.M.; Zhai, D.G.; Wang, Y.H.; Zhang, S.; Sha, Y.Z.; Liu, G.; Wu, J. The Guangshigou uranium deposit, northern Qinling Orogen, China: A product of assimilation-fractional crystallization of pegmatitic magma. *Ore Geol. Rev.* **2018**, *99*, 17–41. [CrossRef]
25. Lee, R.G.; Byrne, K.; D'Angelo, M.; Hart, C.J.R.; Hollings, P.; Gleeson, S.A.; Alfaro, M. sing zircon trace element composition to assess porphyry copper potential of the Guichon Creek batholith and Highland Valley Copper deposit, south-central British Columbia. *Miner. Depos.* **2021**, *56*, 215–238. [CrossRef]
26. Li, H.; Cao, J.; Algeo, T.J.; Jiang, W.; Liu, B.; Wu, Q. Zircons reveal multi-stage genesis of the Xiangdong (Dengfuxian) tungsten deposit, South China. *Ore Geol. Rev.* **2019**, *111*, 102979. [CrossRef]
27. Wang, L.G.; Li, X.Z.; Yu, X.W.; Zhu, D.C.; Wang, Y.P.; Zhang, W.; Ke, C.H.; Hu, Z.G.; Guo, R.P.; Hao, X.Z. Petrogenesis and tectonic setting of Dazeshan and Tianzhushan granites in Jiaodong peninsula: Geochemistry, zircon U-Pb geochronology and Lu-Hf isotopic constraints. *J. Jilin Univ.* **2022**, *52*, 879–898, (In Chinese with English abstract).
28. Liu, X.L.; Li, W.C. The Indo-Chinese epoch magmatism in Gega arc of Yunnan: Evidence from zircon U-Pb dating and Hf isotopic composition. *Earth Sci. Front.* **2013**, *20*, 57–74, (In Chinese with English abstract).
29. Duan, S.S.; Dong, Y.; Wang, W.Z.; Guo, L. Geochronology, geochemistry and Hf isotopic characteristics of Early Cretaceous A-Type granite in Erdene area, southern Mongolia and their geological significance. *J. Jilin Univ.* **2022**, *52*, 917–929, (In Chinese with English abstract).
30. Deng, J.; Wang, Q.F.; Li, G.J.; Li, C.S.; Wang, C.M. Tethys tectonic evolution and its bearing on the distribution of important mineral deposits in the Sanjiang region, SW China. *Gondwana Res.* **2014**, *26*, 419–437. [CrossRef]
31. Li, B.; Wang, X.F.; Yue, Y.; Huang, Z.L.; Tang, G.; Liu, Y.D.; Zou, G.F.; Xiang, Z.P. Ore-field structural system and its mechanism of rock-and ore-controlling processes of Yangla Cu deposit in northwest Yunnan, China. *Chin. J. Nonferrous Met.* **2021**, *31*, 2596–2611, (In Chinese with English abstract).
32. Li, B.; Zou, G.F.; Wen, S.M.; Huang, Z.L.; Tang, G.; Liu, Y.D.; Sheng, R. Fault structure, ore-controlling structural model and prospecting prediction of Yangla copper deposit, northwestern Yunnan. *Miner. Explor.* **2014**, *5*, 699–711, (In Chinese with English abstract).

33. Chen, K.X.; Wei, J.Q.; Yan, D.P.; Fan, Y.H. A preliminary study of porphyry bodies and related mineralizaton in Yangla area, Deqing, western Yunnan. *Geol. Miner. Resour. S. China* **1999**, *2*, 1–81, (In Chinese with English abstract).
34. Lu, Y.F.; Zhan, M.G.; Chen, K.X. U-Pb isotopic dating of basalt from the Gajinxueshan Group in the Jinshajiang tectonic belt. *Reg. Geol. China* **2000**, *19*, 155–158, (In Chinese with English abstract).
35. Zeng, P.S.; Wang, Y.B.; Ma, J.; Wang, Z.Q.; Wen, L.G. Diachronous collision-closure of the Jinshajiang paleo-ocean basin in the Yangla area: Constraints from the ages of the granites. *Earth Sci. Front.* **2018**, *25*, 92–105, (In Chinese with English abstract).
36. Wu, Y.B.; Zheng, Y.F.; Gong, B.; Tang, J.; Zhao, Z.F.; Zha, X.P. Zircon U-Pb ages and oxygen isotope compositions of the Luzhenguan magmatic complex in the Beihuaiyang zone. *Acta Petrol. Sin.* **2004**, *20*, 1007–1024, (In Chinese with English abstract).
37. Williams, I.S.; Claesson, S. Isotopic evidence for the Precambrian provenance and Cale-donian metamorphism of high grade paragneisses from the Seve Nappes, Scandi-navian Caledonides. *Contrib. Mineral. Petrol.* **1987**, *97*, 196–204. [CrossRef]
38. Yuan, H.L.; Gao, S.; Liu, X.M.; Li, H.M.; Günther, D.; Wu, F.Y. Accurate U-Pb age and trace element determinations of zircon by laser ablation-inductively coupled plasma-mass spectrometry. *Geostand. Geoanalytical Res.* **2010**, *28*, 353–370. [CrossRef]
39. Jackson, S.E.; Pearson, N.J.; Griffin, W.L.; Belousova, W.A. The application of laser ablation-inductively coupled plasma-mass spectrometry to in situ U-Pb zircon geochronology. *Chem. Geol.* **2004**, *211*, 47–69. [CrossRef]
40. Li, X.H.; Long, W.G.; Li, Q.L.; Liu, Y.; Zheng, Y.F.; Yang, Y.H.; Chamberlain, K.R.; Wan, D.F.; Guo, C.H.; Wang, X.C.; et al. 2010 Penglai zircon megacrysts: A potential new working reference material for microbeam determination of Hf-O isotopes and U-Pb age. *Geostand. Geoanalytical Res.* **2010**, *34*, 117–134. [CrossRef]
41. Li, X.H.; Tang, G.Q.; Gong, B.; Yang, Y.H.; Hou, K.J.; Hu, Z.C.; Li, Q.L.; Liu, Y.; Li, W.X. Qinghu zircon: A working reference for microbeam analysis of U-Pb age and Hf and O isotopes. *Chin. Sci. Bull.* **2013**, *58*, 1954–1961. [CrossRef]
42. Sláma, J.; Košler, J.; Condon, D.J.; Crowley, J.L.; Gerdes, A.; Hanchar, J.M.; Horstwood, M.S.A.; Morris, G.A.; Nasdala, L.; Norberg, N.; et al. Pleovice zircon—A new natural reference material for U-Pb and Hf isotopic microanalysis. *Chem. Geol.* **2008**, *249*, 1–35. [CrossRef]
43. Münker, C.; Weyer, S.; Scherer, E.; Mezger, K. Separation of high field strength elements (Nb, Ta, Zr, Hf) and Lu from rock samples for MC-ICPMS measurements. *Geochem. Geophys. Geosystems* **2001**, *2*. [CrossRef]
44. Amelin, Y.; Lee, D.C.; Halliday, A.N.; Pidgeon, R.T. Nature of the Earth's earliest crust from hafnium isotopes in single detrital zircons. *Nature* **1999**, *399*, 252–255. [CrossRef]
45. Griffin, W.L.; Pearson, N.J.; Belousova, E.; Jackson, S.E.; Achterbergh, E.V.; O'reilly, S.Y.; Shee, S.R. The Hf isotope composition of cratonic mantle: LAM-MC-ICPMS analysis of zircon megacrysts in kimberlites. *Geochim. Cosmochim. Acta* **2000**, *64*, 133–147. [CrossRef]
46. Griffin, W.; Wang, X.; Jackson, S.E.; Pearson, N.J.; O'Reilly, S.Y.; Xu, X.S.; Zhou, X.M. Zircon chemistry and magma mixing, SE China: In-situ analysis of Hf isotopes, Tonglu and Pingtan igneous complexes. *Lithos* **2002**, *61*, 237–269. [CrossRef]
47. Hoskin, P.W.O. Trace-element composition of hydrothermal zircon and the alteration of hadean zircon from the Jack Hills, Australia. *Geochim. Cosmochim. Acta* **2005**, *69*, 637–648. [CrossRef]
48. Hoskin, P.W.O.; Schaltegger, U. The composition of zircon and igneous and metamorphic petrogenesis. *Petrogenesis* **2003**, *53*, 27–62.
49. Viala, M.; Hattori, K. Hualgayoc mining district, northern Peru: Testing the use of zircon composition in exploration for porphyry-type deposits. *J. Geochem. Explor.* **2021**, *223*, 106725. [CrossRef]
50. Xia, Q.; Li, Y.S.; Li, X.F.; Kou, Y.C. Zircon U-Pb ages, trace elements and Hf isotopes of the mineralized granodiorite dikes in the Anfangba gold deposit, west Qinling. *Acta Petrol. Sin.* **2021**, *37*, 1713–1730, (In Chinese with English abstract).
51. Li, H.; Watanabe, K.; Yonezu, K. Zircon morphology, geochronology and trace element geochemistry of the granites from the Huangshaping polymetallic deposit, South China: Implications for the magmatic evolution and mineralization processes. *Ore Geol. Rev.* **2014**, *60*, 14–35. [CrossRef]
52. Rubatto, D. Zircon trace element geochemistry: Partitioning with garnet and the link between U–Pb ages and metamorphism. *Chem. Geol.* **2002**, *184*, 123–138. [CrossRef]
53. Sun, S.S.; Mcdonough, W.F. Chemical and isotope systematics of oceanic basalts: Implications for mantle composition and processes. *Geol. Soc. Spec. Publ.* **1989**, *4*, 313–345. [CrossRef]
54. Amelin, Y.; Lee, D.C.; Halliday, A.N. Early-middle archaean crustal evolution deduced from Lu-Hf and U-Pb isotopic studies of single zircon grains. *Geochim. Cosmochim. Acta* **2000**, *64*, 4205–4225. [CrossRef]
55. Vervoort, J.D.; Patchett, P.J.; Gehrels, G.E.; Nutman, A.P. Constraints on early Earth differentiation from hafnium and neodymium isotopes. *Nature* **1996**, *379*, 624–627. [CrossRef]
56. Blichert-Toft, J.; Albarede, F. The Lu-Hf isotope geochemistry of chondrites and the evolution of the mantle-crust system. *Earth Planet. Sci. Lett.* **1997**, *148*, 243–258. [CrossRef]
57. Zhu, Y.H.; Xu, D.R.; Zhang, J.W.; He, M.L.; Chen, G.W.; Shan, Q.; Wang, Z.L. Geochronology and Source Characteristics of the Shimenshan Molybdenum Polymetallic Deposit in Hainan Island and Its Implications for Mineralization by Magmatic Oxygen Fugacity. *Geotecton. Metallog.* **2022**. [CrossRef]
58. Watson, E.B.; Harrison, T.M. Zircon saturation revisited: Temperature and composition effects in a variety of crustal magma types. *Earth Planet. Sci. Lett.* **1983**, *64*, 295–304. [CrossRef]
59. Watson, E.B.; Wark, D.A.; Thomas, J.B. Crystallization thermometers for zircon and rutile. *Contrib. Mineral. Petrol.* **2006**, *151*, 413. [CrossRef]

60. Ferry, J.M.; Watson, E.B. New thermodynamic models and revised calibrations for the Ti-in-zircon and Zr-in-rutile thermometers. *Contrib. Mineral. Petrol.* **2007**, *154*, 429–437. [CrossRef]
61. Hayden, L.A.; Watson, E.B. Rutile saturation in hydrous siliceous melts and its bearing on Ti-thermometry of quartz and zircon. *Earth Planet. Sci. Lett.* **2007**, *258*, 561–568. [CrossRef]
62. Zou, X.Y.; Qin, K.Z.; Han, X.L.; Li, G.M.; Evans, N.J.; Li, Z.Z.; Yang, W. Insight into zircon REE oxy-barometers: A lattice strain model perspective. *Earth Planet. Sci. Lett.* **2019**, *506*, 87–96. [CrossRef]
63. Trail, D.; Watson, E.B.; Tailby, N.D. Ce and Eu anomalies in zircon as proxies for the oxidation state of magmas. *Geochim. Cosmochim. Acta* **2012**, *97*, 70–87. [CrossRef]
64. Chelle-Michou, C.; Chiaradia, M.; Ovtcharova, M.; Ulianov, A.; Wotzlaw, J.F. Zircon petrochronology reveals the temporal link between porphyry systems and the magmatic evolution of their hidden plutonic roots (the Eocene Coroccohuayco Deposit, Peru). *Lithos* **2014**, *198–199*, 129–140. [CrossRef]
65. Smythe, D.J.; Brenan, J.M. Magmatic oxygen fugacity estimated using zirconmelt partitioning of cerium. *Earth Planet. Sci. Lett.* **2016**, *453*, 260–266. [CrossRef]
66. Zhang, C.C.; Sun, W.D.; Wang, J.T.; Zhang, L.P.; Sun, S.J.; Wu, K. Oxygen fugacity and porphyry mineralization: A zircon perspective of Dexing porphyry Cu deposit, China. *Geochim. Cosmochim. Acta* **2017**, *206*, 343–363. [CrossRef]
67. Li, S.K.; Liu, X.L.; Lv, Y.X.; Zhang, S.T.; Liu, S.H.; Chen, J.H.; Li, Z.H.; Yu, H.J.; Zhang, C.Y. Indication of Zircon oxygen fugacity to different mineralization control factors of porphyry deposits in Zhongdian ore-concentrated area, southern Yidun arc. *Earth Sci.* **2022**, *47*, 1435–1458, (In Chinese with English abstract).
68. Loucks, R.R.; Fiorentini, M.L.; Henríquez, G.J. New magmatic oxybarometer using trace elements in zircon. *J. Petrol.* **2020**, *61*, egaa034. [CrossRef]
69. Xu, M.; Duan, X.X.; Chen, B.; Wang, Z.Q.; Chen, Y.J.; Li, X.F. Trace elements in zircon: Constrain on magmatic differentiation-A case study on Triassic Wangxianling granitoid in southern Hunan Province. *Geol. Rev.* **2020**, *66*, 665–685, (In Chinese with English abstract).
70. Xiong, X.; Zhu, L.M.; Zhang, G.W.; Li, N.; Yuan, H.L.; Ding, L.L.; Sun, C.; Guo, A.L. Fluid inclusion geochemistry and magmatic oxygen fugacity of the Wenquan Triassic molybdenum deposit in the Western Qinling Orogen, China. *Ore Geol. Rev.* **2018**, *99*, 244–263. [CrossRef]
71. Li, H.; Wu, J.H.; Evans, N.J.; Jiang, W.C.; Zhou, Z.K. Zircon geochronology and geochemistry of the Xianghualing A-type granitic rocks: Insights into multi-stage Sn-polymetallic mineralization in South China. *Lithos* **2018**, *312–313*, 1–20. [CrossRef]
72. Li, H.; Li, J.W.; Algeo, T.J.; Wu, J.H.; Cisse, M. Zircon indicators of fluid sources and ore genesis in a multi-stage hydrothermal system: The Dongping Au deposit in North China. *Lithos* **2018**, *314–315*, 463–478. [CrossRef]
73. Ye, L.X.; Zhang, D.Y.; Wang, F.Y.; Jiang, Z.R.; Chen, X.F.; Zhang, F.; Xi, X.C.; Zhou, T.F. Magmatic genesis and mineralization potential of Qingyang—Jiuhuashan complex pluton: Evidence from zircon Hf isotopes and trace elements. *Geol. Rev.* **2022**, *68*, 1278–1300, (In Chinese with English abstract).
74. Bolhar, R.; Weaver, S.D.; Whitehouse, M.J.; Palin, J.M.; Woodhead, J.D.; Cole, J.W. Sources and evolution of arc magmas inferred from coupled O and Hf isotope systematics of plutonic zircons from the Cretaceous Separation Point Suite (New Zealand). *Earth Planet. Sci. Lett.* **2008**, *268*, 312–324. [CrossRef]
75. Wang, L.G.; Zhu, D.C.; Guo, R.M.; Yu, X.W.; Tian, J.X.; Ke, C.H.; Liu, H.D.; Tian, R.C.; Gao, H.L. Geochemistry, zircon U-Pb age and Lu-Hf isotopes of the Cangshang and Sanshandao monzogranites in the Northwestern Jiaodong Peninsula, China. *Acta Geol. Sin.* **2018**, *92*, 2081–2095, (In Chinese with English abstract).
76. Hou, M.L.; Jiang, Y.H.; Jiang, S.Y.; Ling, H.F.; Zhao, K.D. Contrasting origins of late Mesozoic adakitic granitoids from the northwestern Jiaodong Peninsula, east China: Implications for crustal thickening to delamination. *Geol. Mag.* **2007**, *144*, 619–631. [CrossRef]
77. Kemp, A.I.S.; Hawkesworth, C.J.; Foster, G.L.; Paterson, B.A.; Woodhead, J.D.; Hergt, J.M.; Gray, C.M.; Whitehouse, M.J. Magmatic and crustal differentiation history of granitic rocks from Hf-O isotopes in zircon. *Science* **2007**, *315*, 980–983. [CrossRef]
78. Li, Y.J.; Wei, J.H.; Chen, H.Y.; Li, H.; Chen, C.; Hou, B.J. Petrogenesis of the Xiasai early Cretaceous A-type granite from the Yidun island arc belt, SW China: Constraints from zircon U-Pb age, geochemistry and Hf isotope. *Geotecton. Metallog.* **2014**, *38*, 939–953, (In Chinese with English abstract).
79. Wang, N.; Wu, C.L.; Qin, H.P.; Lei, M.; Guo, W.F.; Zhang, X.; Chen, H.J. Zircon U-Pb geochronology and Hf isotopic characteristic of the Daocheng granite and Haizishan granite in the Yidun Arc, western Sichuan, and their geological significance. *Acta Geol. Sin.* **2016**, *90*, 3227–3245, (In Chinese with English abstract).
80. Zhang, R.G.; Gao, X.; Yang, L.Q. Identification of magma mixing: A case study of the Daocheng batholith in the Yidun Arc. *Adv. Earth Sci.* **2018**, *33*, 1058–1074.
81. Yang, D.T.; Wang, Y.B. Detrital zircon LA-MC-ICP-MS U-Pb age and provenance characteristics of ore-hosting rocks in Yangla copper deposit, Northwestern Yunnan. *Geol. Rev.* **2013**, *59*, 1131–1142, (In Chinese with English abstract).
82. Greentree, M.R.; Li, Z.X.; Li, X.H.; Wu, H.C. Late Mesoproterozoic to earliest Neoproterozoic basin record of the Sibao orogenesis in western South China and relationship to the assembly of Rodinia. *Precambrian Res.* **2006**, *151*, 79–100. [CrossRef]
83. Zhao, X.F.; Zhou, M.F.; Hitzman, M.W. Late paleoproterozoic to early mesoproterozoic tangdan sedimentary rockhosted stratabound copper deposit, Yunnan Province, Southwest China. *Econ. Geol.* **2012**, *107*, 357–375. [CrossRef]

84. Zhao, J.H.; Zhou, M.F.; Yan, D.P.; Yang, Y.H.; Sun, M. Zircon Lu-Hf isotopic constraints on Neoproterozoic subduction-related crustal growth along the western margin of the Yangtze Block, South China. *Precambrian Res.* **2008**, *163*, 189–209. [CrossRef]
85. Wu, F.Y.; Li, X.H.; Yang, J.H.; Zheng, Y.F. Discussions on the petrogenesis of granites. *Acta Petrol. Sin.* **2007**, *23*, 1217–1238, (In Chinese with English abstract).
86. Li, X.H.; Li, W.X.; Wang, X.C.; Li, Q.L.; Liu, Y.; Tang, G.Q. Role of mantle-derived magma in genesis of early Yanshanian granites in the Nanling Range, South China: In situ zircon Hf-O isotopic constraints. *Sci. China Ser. D Earth Sci.* **2009**, *39*, 872–887. [CrossRef]
87. Bell, E.A.; Kirkpatrick, H.M. Effects of crustal assimilation and magma mixing on zircon trace element relationships across the Peninsular Ranges Batholith. *Chem. Geol.* **2021**, *586*, 120616. [CrossRef]
88. Valley, J. Oxygen isotopes in zircon. *Rev. Mineral. Geochem.* **2003**, *53*, 343–385. [CrossRef]
89. Trail, D.; Tailby, N.D.; Sochko, M.; Ackerson, M.R. Possible biosphere-lithosphere interactions preserved in igneous zircon and implications for Hadean earth. *Astrobiology* **2015**, *15*, 575–586. [CrossRef]
90. Zhu, Z.; Campbell, I.H.; Allen, C.M.; Burnham, A.D. S-type granites: Their origin and distribution through time as determined from detrital zircons. *Earth Planet. Sci. Lett.* **2020**, *536*, 116140. [CrossRef]
91. Bell, E.A.; Boehnke, P.; Barboni, M.; Harrison, T.M. Tracking chemical alteration in magmatic zircon using rare earth element abundances. *Chem. Geol.* **2019**, *510*, 56–71. [CrossRef]
92. Morton, D.M.; Miller, F.K.; Kistler, R.W.; Premo, W.R.; Lee, C.T.A.; Langenheim, V.E.; Cossette, P. Framework and petrogenesis of the northern Peninsular Ranges batholith, southern California. Peninsular Ranges Batholith, Baja California and Southern California. *Geol. Soc. Am. Mem.* **2014**, *211*, 61–143.
93. Kistler, R.W.; Wooden, J.L.; Premo, W.R.; Morton, D.M.; Miller, F.K. Pb–Sr–Nd–O isotopic characterization of Mesozoic rocks throughout the northern end of the Peninsular Ranges batholith: Isotopic evidence for the magmatic evolution of oceanic arc–continental margin accretion during the Late Cretaceous of southern California. Peninsular Ranges Batholith, Baja California and Southern California. *Geol. Soc. Am. Mem.* **2014**, *211*, 263–316.
94. Bruand, E.; Storey, C.; Fowler, M. Accessory mineral chemistry of high Ba-Sr granites from northern Scotland: Constraints on petrogenesis and records of whole-rock signature. *J. Petrol.* **2014**, *55*, 1619–1651. [CrossRef]
95. Belousova, E.; Griffin, W.; O'Reilly, S.Y.; Fisher, N. Igneous zircon: Trace element composition as an indicator of source rock type. *Contrib. Mineral. Petrol.* **2002**, *143*, 602–622. [CrossRef]
96. Lee, R.G.; Dilles, J.H.; Tosdal, R.M.; Wooden, J.L.; Mazdal, F.K. Magmatic evolution of granodiorite intrusions at the El Salvador porphyry copper deposit, Chile, based on trace element composition and U/Pb age of zircons. *Econ. Geol.* **2017**, *112*, 245–273. [CrossRef]
97. Shen, P.; Hattori, K.; Pan, H.D.; Jackson, S.; Seitmuratova, E. Oxidation condition and metal fertility of granitic magmas: Zircon trace-element data from porphyry Cu deposits in the central Asian orogenic belt. *Econ. Geol.* **2015**, *110*, 1861–1878. [CrossRef]
98. Geng, T.; Zhou, Y.Z.; Li, X.Y.; Wang, J.; Chen, C.; Wang, K.Y.; Han, Z.Q. The discrimination between ore-forming and barren granites based on zircon REE compositions: Insights from big data mining. *Geol. Bull. China* **2019**, *38*, 1992–1998, (In Chinese with English abstract).
99. Yang, X.B.; Wang, X.F.; Li, B.; Liu, Y.D.; Liu, C.C.; Liu, F.Z.; Huang, Z.L.; Hu, D.P. Discovery of tungsten orebody in the depth of the Yangla large Cu deposit, northwest Yunnan. *Acta Mineral. Sin.* **2022**, *42*, 1–4. [CrossRef]
100. Veksler, I.V.; Dorfman, A.M.; Kamenetsky, M.; Dulski, P.; Dingwell, D.B. Partitioning of lanthanides and Y between immiscible silicate and fluoride melts, fluorite and cryolite and the origin of the lanthanide tetrad effect in igneous rocks. *Geochim. Cosmochim. Acta* **2005**, *69*, 2847–2860. [CrossRef]
101. Fulmer, E.C.; Nebel, O.; Westrenen, W.V. High-precision high field strength element partitioning between garnet, amphibole and alkaline melt from Kakanui, New Zealand. *Geochim. Cosmochim. Acta* **2010**, *74*, 2741–2759. [CrossRef]
102. Mao, J.W.; Wu, S.H.; Song, S.W.; Dai, P.; Xie, G.Q.; Su, Q.W.; Liu, P.; Wang, X.G.; Yu, Z.Z.; Chen, X.Y.; et al. The world-class Jiangnan tungsten belt: Geological characteristics, metallogeny, and ore deposit model. *Chin. Sci. Bull.* **2020**, *65*, 3746–3762, (In Chinese with English abstract). [CrossRef]
103. Zhang, J.B.; An, F. Methods for estimating magma oxidation state of porphyry copper deposits: A review. *Miner. Depos.* **2018**, *37*, 1052–1064, (In Chinese with English abstract).